The role of slabs and oceanic plate geometry in the net rotation of the lithosphere, trench motions, and slab return flow

M. Gérault

Department of Earth Sciences, University of Southern California, 3651 Trousdale Parkway, Los Angeles, California 90089-0740, USA (gerault@usc.edu)

Géosciences Rennes, UMR 6118, Université de Rennes 1, Campus de Beaulieu, F-35042 Rennes CEDEX, France

T. W. Becker

Department of Earth Sciences, University of Southern California, 3651 Trousdale Parkway, Los Angeles, California 90089-0740, USA (twb@usc.edu)

B. J. P. Kaus

Department of Earth Sciences, University of Southern California, 3651 Trousdale Parkway, Los Angeles, California 90089-0740, USA

Institute of Geosciences, University of Mainz, J.J. Becherweg 21, D-55099 Mainz, Germany (kaus@uni-mainz.de)

C. Faccenna

Dipartimento di Scienze Geologiche, Università di Roma Tre, Largo S. Leonardo Murialdo 1, I-00146 Rome, Italy (faccenna@uniroma3.it)

L. Moresi

School of Mathematical Sciences and School of Geosciences, Monash University, Clayton, Victoria 3800, Australia (louis.moresi@monash.edu)

L. Husson

Géosciences Rennes, UMR 6118, Université de Rennes 1, Campus de Beaulieu, F-35042 Rennes CEDEX, France (laurent.husson@univ-rennes1.fr)

Laboratoire de Planétologie et Géodynamique, UMR CNRS 6112, Université de Nantes, F-44322 Nantes, France

[1] Absolute plate motion models with respect to a deep mantle reference frame (e.g., hot spots) typically contain some net rotation (NR) of the lithosphere. Global mantle flow models for the present-day plate setting reproduce similarly oriented NRs but with amplitudes significantly smaller than those found in some high NR Pacific hot spot reference frames. It is therefore important to understand the mechanisms of NR excitation, which we attempt here with two-dimensional cylindrical models of an idealized Pacific domain. We study the influence of slab properties, oceanic ridge position, continental keels, and a weak asthenospheric layer on NR and trench migration. Fast slab return flow develops in models with stiff slabs and moderate slab dips. Rapid NRs, comparable to the high NR Pacific hot spot reference frames, are

primarily induced by asymmetric slab dips, in particular a shallow slab beneath South America and a steep slab in the western Pacific. A scaling relationship links the amplitude of NR to plate size, slab dip angle, and slab viscosity. Asymmetric ridge positions also promote NR through asymmetric plate sizes. Continental keels have less impact, in contrast to what has been found in earlier global studies. Several models yield unidirectional Pacific trench motions, such as slab advance in the western Pacific and, simultaneously, slab retreat in the eastern Pacific. Our model provides a physical explanation for NR generation in the present-day Pacific setting and hints at mechanisms for the temporal evolution of the basin.

1. Introduction

[2] Absolute plate motions can be determined by expressing relative plate motions in a deep mantle reference frame, usually based on hot spots [e.g., *Morgan*, 1971; *Minster et al.*, 1974; *Torsvik et al.*, 2010]. Absolute plate motions may contain a component that corresponds to a rigid rotation of the surface as a whole, called the net rotation (NR) of the lithosphere. The net rotation is defined as the integral of the crustal velocities over the surface of the Earth, that is, the degree one of the toroidal component of the surface velocity field [e.g., *Ricard et al.*, 1991; *O'Connell et al.*, 1991].
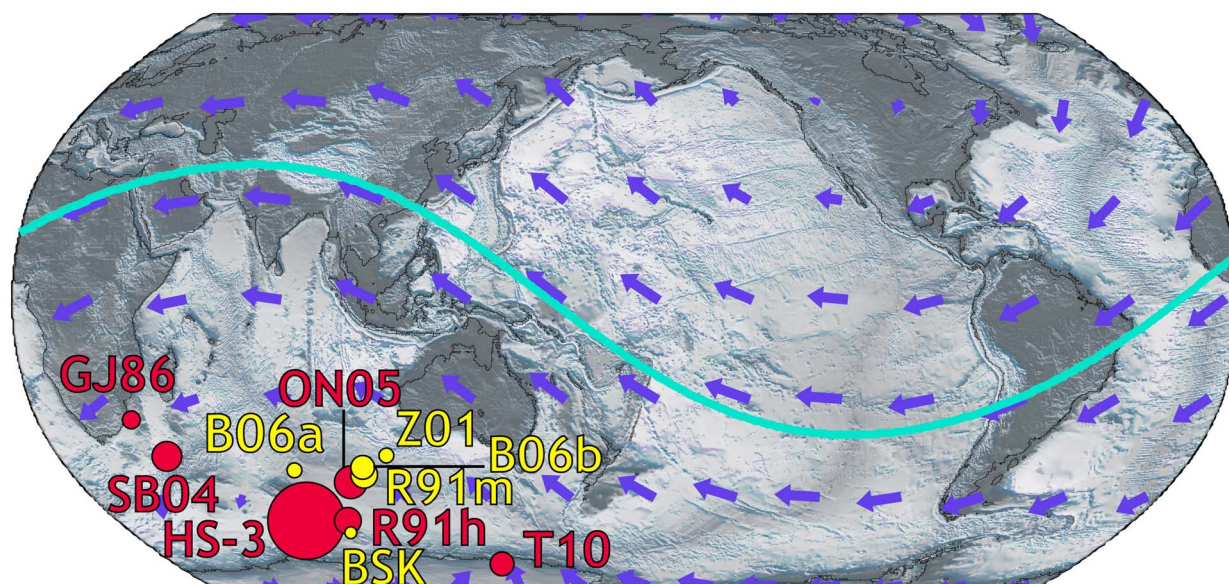
[3] While NR is an ubiquitous feature of absolute plate velocity reference frames, its amplitude may vary significantly between models. For the present day, many reference frames [e.g., *Gordon and Jurdy*, 1986; *Ricard et al.*, 1991; *Gripp and Gordon*, 2002; *Steinberger et al.*, 2004; *Torsvik et al.*, 2010], however, indicate a NR Euler pole of net rotation located in the Southwest Indian Ocean (Figure 1). While not the fastest suggested NR [*Crespi et al.*, 2007], the Pacific hot spot reference frame HS-3 [*Gripp and Gordon*, 2002] contains the largest NR in the most widely used reference frames (NR rate of $0.44°/Myr$, i.e., a maximum velocity of 4.9 cm/yr). The majority of the other reference frames contains a NR rate of less than $0.2°/Myr$. A recent update of HS-3 [*Zheng et al.*, 2010] argues for a lower amplitude of $\sim0.35°/Myr$.

[4] *Becker* [2008a, 2008b] suggested that azimuthal anisotropy from surface waves imposes an upper bound for NR rates, which, together with consistent findings for shear wave splitting [*Kreemer*, 2009; *Conrad and Behn*, 2010] implies that only an amplitude of about half the NR contained in HS-3 is globally permissible. On the other hand, *Alpert et al.* [2010] found that the shear induced by the large NR contained in HS-3 provides the best fit to slab deformation, as suggested by *Uyeda and Kanamori* [1979] and *Doglioni et al.* [2007].

[5] The choice of an appropriate absolute reference frame is key in validating geodynamic models for the motions of the oceanic trenches, for example. Trench motions give insight into the force balance along plate margins and into subduction dynamics [e.g., *Billen*, 2008; *Becker and Faccenna*, 2009], and are dependent on the choice of an absolute reference frame [e.g., *Funiciello et al.*, 2008; *Schellart et al.*, 2008; *Di Giuseppe et al.*, 2009], and so is the correlation between lowermost mantle seismic anomalies and subduction history [e.g., *Ricard et al.*, 1993; *Steinberger*, 2000; *van der Meer et al.*, 2010]. Therefore, in order to better understand plate dynamics, it is crucial to determine a consistent range of net rotation amplitudes, which could potentially guide the choice of an absolute terrestrial reference frame. More generally, the physical mechanisms for producing NR remain unclear. We attempt to elucidate some of these mechanisms in this paper.

[6] Plate motions are typically considered to arise from mantle convection [e.g., *Turcotte and Oxburgh*, 1967], driven by buoyancy forces resulting from density anomalies. These anomalies generate a

Figure 1. Euler poles of net rotation contained in different absolute plate motions reference frames (red) and geodynamic models (yellow). The purple vectors and the turquoise curve show the velocity field and the equator of the net rotation in HS-3. Plate model abbreviations are as follows: GJ86, *Gordon and Jurdy* [1986]; HS-3, *Gripp and Gordon* [2002]; ON05, *O'Neill et al.* [2005]; R91h, *Ricard et al.* [1991]; SB04, *Steinberger et al.* [2004]; T10, *Torsvik et al.* [2010]. Geodynamic model abbreviations are as follows: B06a, B06b, BSK, *Becker* [2006]; R91m, *Ricard et al.* [1991]; Z01, *Zhong* [2001].

poloidal flow field in a medium where the viscosity is uniform or radially stratified. However, lateral variations of viscosity (LVVs) are required for body forces to induce a toroidal flow field [e.g., *Ricard and Vigny*, 1989; *O'Connell et al.*, 1991; *Ricard et al.*, 1991; *Ribe*, 1992; *Bercovici et al.*, 2000] and generate realistic surface velocities, composed of both poloidal (divergent-convergent) and toroidal (strike-slip) components [*Hager and O'Connell*, 1978]. The viscosity stratification also influences NR, in particular a stiff lower mantle [*Ricard et al.*, 1991], which channels the flow into the upper mantle. This reinforces the effect of the LVVs that may be most pronounced in the upper few hundred kilometers [*Zhong*, 2001; *Becker*, 2006].

[7] Tidal drag has been proposed as a major plate driving mechanism inducing NR [e.g., *Wegener*, 1924; *Bostrom*, 1971; *Scoppola et al.*, 2006]. However, *Jordan* [1974], *Ricard et al.* [1991], and *Ranalli* [2000] demonstrated that this hypothesis is incompatible with current estimates of upper mantle viscosities. Furthermore, the orientation of the net rotation of the lithosphere is believed to have varied over the past 150 Ma [*Torsvik et al.*, 2010], and so has its amplitude to a smaller extent. This suggests that the net rotation has tectonic origins, and does not result from a perpetual external forcing.

[8] The thin sheet model of *Ricard et al.* [1991] included LVVs between suboceanic and subcontinental mantle, and predicted a net rotation with a maximum amplitude of 1.7 cm/yr and a Euler pole located in the Southern Indian Ocean, both of which match the predictions of some hot spot reference frames well. Thus, these authors have suggested that NR results from a differential plate-mantle coupling between oceanic and continental plates. This is supported by seismological data, which suggest that continents have deep, potentially stiff structures underneath them, while low-velocity zones can be detected underneath oceanic plates [e.g., *Jordan*, 1975, 1988]. After earlier models with LVVs failed to produce significant NR [*Zhang and Christensen*, 1993; *Čadek et al.*, 1997; *Wen and Anderson*, 1997], the models with stiff keels by *Zhong* [2001] and *Becker* [2006] successfully predicted the sense of the net rotation (Figure 1). However, these authors obtained maximum NR amplitudes only up to 0.13°/Myr [*Becker*, 2006], which is toward the lower end of those contained in plate models but consistent with the upper bound of *Becker* [2008a, 2008b].

[9] Given these discrepancies in global models, we consider it useful to study the influence of regional dynamics. Two properties control how much a plate can contribute to NR: its size, and its velocity. At

present, driving mechanisms of NR and the dynamics of the Pacific region are intrinsically related. Several recent studies have been focusing on the Pacific, where most trenches are located. They attempt to explain trench and plate motions either by invoking ridge (spreading center) position [*Nagel et al.*, 2008], gravitational potential energy (GPE) variations induced by the Andes [*Husson et al.*, 2008], or showing the effect of a cratonic keel in the vicinity of a subducting slab [*O'Driscoll et al.*, 2009]. Stiff continental keels [e.g., *Conrad and Lithgow-Bertelloni*, 2006; *van Summeren et al.*, 2012] have been found to contribute to the net rotation in 3-D numerical computations [*Zhong*, 2001; *Becker*, 2006] in the absence of a low-viscosity layer underneath them. *Gurnis and Torsvik* [1994] showed in a 2-D numerical model that the presence of continental keels can significantly influence continental plate motions when the plate driving mechanism arises "from below", in the case of an upwelling, for example. However, when slabs and ridges drive the plates as expected for present-day tectonics, they found that continental keels have a minor effect. Slab dip angles in the Pacific are generally asymmetric on each side of the basin, along the equator of NR, and along great circles parallel to this path [e.g., *Uyeda and Kanamori*, 1979; *Heuret and Lallemand*, 2005; *Li et al.*, 2008]. Subducting slabs are known to exert a first order control on plate motions [e.g., *Forsyth and Uyeda*, 1975; *Lithgow-Bertelloni and Richards*, 1998; *Becker and O'Connell*, 2001; *Conrad and Lithgow-Bertelloni*, 2002], although the intensity and pathway through which the pull is transmitted to the plates remains debated [e.g., *Conrad and Lithgow-Bertelloni*, 2004; *Becker*, 2006; *Capitanio et al.*, 2009]. For example, differences between oceanic and continental plate speeds are a consequence of LVVs [e.g., *Čadek and Fleitout*, 2003; *Becker*, 2006], but also naturally arise on each side of a subduction zone from one-sided slab pull versus viscous slab suction [*Conrad and Lithgow-Bertelloni*, 2002]. Asymmetric slab dip angles on each side of the Pacific basin may induce an asymmetry in effective slab pull forces and in the coupling between plates and mantle.

[10] It has been suggested that asymmetric slab dip angles result from the net rotation itself [e.g., *Uyeda and Kanamori*, 1979; *Doglioni et al.*, 2007; *Husson et al.*, 2008]. However, *Lallemand et al.* [2005] found only a small difference between the average dip of western versus eastern dipping slab. They suggested that western dipping slabs are a few degrees steeper on average because the overriding plate is often oceanic, a correlation that is confirmed by subduction zones that are dipping neither westward nor eastward. Several studies suggest that slab dip angles can also be matched without invoking any NR. For instance, the kinematic models by *Hager and O'Connell* [1978], which account for plate motions in a no-net-rotation (NNR) reference frame, can accurately predict slab dip angles at several locations. *Faccenna et al.* [2007] have also suggested that slab dip angles are controlled first by regional mantle dynamics and plate properties.

[11] Lithospheric rheology, effective viscosity, and the amount of weakening that slabs undergo as they subduct is a matter of debate (cf. discussion by *Billen* [2008] and *Becker and Faccenna* [2009]), yet it is key to applying the predictions of numerical models to the Earth. The weak zones required between the plates to obtain plate-like motions [e.g., *King and Hager*, 1990; *Olson and Bercovici*, 1991], while being among the strongest LVVs and generating other harmonic degrees of toroidal flow [e.g., *Tackley*, 2000a, 2000b], seem to excite little net rotation [*Zhong*, 2001].

[12] In this paper, we explore all of the aforementioned effects in an idealized model. We assume that past tectonic events shaped the morphology of the plates and slabs as observed at present. We show numerically that plate geometry, slab viscosity, and slab dip angles may induce rapid NR, and a westward motion of the trenches surrounding the Pacific.

2. Model

2.1. Physical Parameters and Geometric Variables

[13] Our model is intended to mimic the Pacific domain and the surrounding plates along a schematic cross section of the Earth, along the equator of the net rotation, which crosses the Pacific from southeast to northwest. The representation of Africa and Eurasia is simplified to a single continental plate referred to as Eurasia, and the Philippine plate is omitted. Therefore, four plates and two ridges are represented in the model. By modeling the lithosphere along the equator of the NR, the goal is to understand how plate geometry controls the amplitude of the NR (its direction being fairly well agreed upon) and trench kinematics. Model parameters are given Table 1. The variables of interest are illustrated in Figure 2, where the asymmetric position of the East Pacific Rise and the length of

Table 1. Model Parameters

Parameter Description	Value (kg/m³)
Upper and lower mantle density	3,200
Continental lithosphere density	3,200
Continental keels density	3,200
Slabs and oceanic lithosphere density	3,280
Upwelling density	3,170

Parameter Description	Value (Pa s)
Upper mantle reference viscosity	10^{20}
Oceanic and continental lithosphere viscosity	$3 \cdot 10^{23}$
Weak zone viscosity (ridge)	10^{19}
Weak zone viscosity (trench)	10^{20}
Asthenosphere viscosity	10^{19}
Lower mantle viscosity	10^{22}
Upwelling viscosity	10^{19}

Parameter Description	Value (km)
Weak zones thickness (ridge)	10
Weak zones thickness (trench)	20
Slab, radius of curvature (cf. *Wu et al.*, 2008)	300
Slab, subducted length	1,200
Continental plate thickness	100
Maximum asthenospheric depth	300
Maximum keel depth	250 or 350
Width of the Pacific oceanic basin	16,000
Eurasia, plate length	16,485
South America, plate length	7,485
Atlantic seafloor length of the plates South America & Eurasia	3,485

the Nazca and Pacific plates respect the actual plate geometry along the equator of the net rotation (a length of 12,000 km for the Pacific and 4,000 km for Nazca).
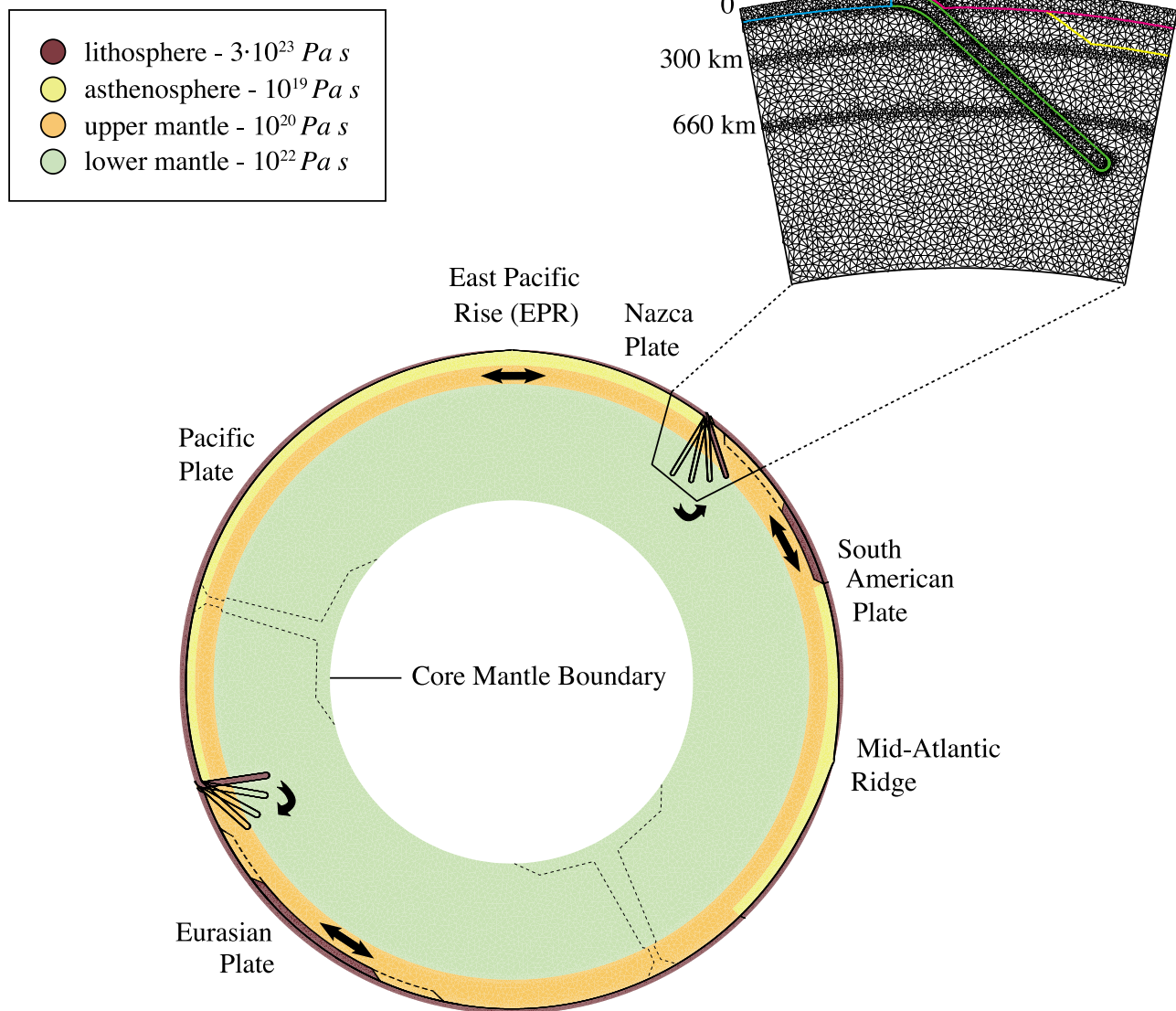
[14] Oceanic plate thickness is defined by $2.32\sqrt{\kappa t}$ from half-space cooling between 0 and 70 Ma, where κ is the thermal diffusivity and t is the age of the plate [*Turcotte and Schubert*, 2002], truncated at a maximum thickness of 110 km. Slab thickness is constant at depth and equal to the plate thickness before it starts bending (Figure 2). The choice of the lithosphere viscosity is guided by the necessity of preventing the plate to stretch excessively, thereby insuring a good "plateness" [*Weinstein and Olson*, 1992; *King et al.*, 1992]. The viscosity of subducting slabs (between the slab hinge and tip) is varied from 10^{20} Pa s (the upper mantle viscosity) to $3 \cdot 10^{23}$ Pa s (the plate viscosity). The goal of using an identical slab length in all models is to use similar body forces as much as possible. This choice results in different slab anchoring into the lower mantle (different portions of the slab enter

the lower mantle) for different slab dip angles, though the slab always extends to, at least, the upper/lower mantle boundary at 660 km. Underneath the oceanic plates, we define a layer one order of magnitude weaker than the upper mantle (the asthenosphere), which creates additional broad scale LVVs. Where specified, the asthenosphere is extended underneath all plates. We also explore the role of continental keels that extend either to 250 km or 350 km, and are neutrally buoyant. Slab dip is varied between 35°, 50°, 65°, and 80°. An example of asymmetric subducting slabs along the equator of NR, on opposite sides of the Pacific basin, is the flat slab subduction below the Central Andes [e.g., *Ramos et al.*, 2002] versus the nearly vertical slab dip angles at the Marianas trench [e.g., *Heuret and Lallemand*, 2005; *Li et al.*, 2008].

2.2. Numerical Setup

[15] Mantle dynamics is modeled by incompressible Stokes flow driven by the oceanic lithosphere at subduction zones that is denser than the rest of the mantle; some models explore the role of upwellings. The behavior of the system is governed by the equations for conservation of mass and momentum, and the constitutive law; here viscosity is assumed to be Newtonian.

[16] Numerical computations are performed using a two-dimensional (2-D) cylindrical finite element model based on a further development of the code MILAMIN [*Dabrowski et al.*, 2008]. We have used a model with a higher mesh resolution at the locations of interest, typically: the plates, the slabs, the keels, and the weak zones. MILAMIN uses the unstructured mesh generator Triangle (J. R. Shewchuk, Triangle, version 1.6, 2007, available at http://www.cs.cmu.edu/ quake/triangle.html) that can be used to adaptively mesh any geometry. The maximum surface area allowed for each, nearly equilateral, triangular element is typically ~40 km² at the surface (i.e., 5 km between two adjacent nodes at the surface), and 300 km² in the lower mantle (Figure 2). The highest resolution that we have used is 500 m between nodes in the weak zones, which corresponds to a minimum element surface area of ~0.4 km². The thinnest weak zone width that we have used is equal to 1 km. The results were stable upon further mesh refinement. Upper and lower boundary conditions are set to free slip, and we display the instantaneous solution for pressure and velocity in a mean nonrotating mantle reference frame, following [*Zhong*, 2001], adapted to 2-D.

Figure 2. Schematic representation of the physical parameters and geometrical variables of the model in an approximate idealization of a cross-Pacific cut through the mantle, close to the equator of the NR pole found in most absolute plate models. The main image shows the viscosity structure used in most models, as well as the geometrical variables (slabs, continental keels, and ridges) and the upwellings (dashed lines) used to test the role of keels. The zoom of the mesh in the top right corner is 10 times coarser than the actual resolution used in the model, where the surface resolution is 10 km. The two lines with higher mesh resolution are the asthenosphere–upper mantle boundary at 300 km depth and upper mantle–lower mantle boundary at 660 km. The colored lines on the mesh inset show the limits of the slab (green), the oceanic lithosphere (blue), a keel (yellow), and the continental lithosphere (pink).

2.3. Measure of Net Rotation in Cylindrical Models

[17] In a 3-D numerical model, the net rotation can simply be computed as the degree one of the toroidal part of the surface velocity field. In 2-D, the only component of the toroidal flow field that develops is a net shear component equivalent to the net rotation, which can be computed as the average of the surface velocities. Stokes flow velocities are typically set by the ratio of density anomalies to viscosity; thus, a global increase or decrease in plate speed may not reflect a change in dynamics. Here, the amount of net surface motion is defined as the ratio of the average surface velocity over the average absolute surface velocity, which we call γ. Such a nondimensional measure shows how the amount of net rotation compares to the average rate of plate motions in the model. For HS-3, $\gamma = 0.83$,

Table 2. Slab Dip and Plate Sizes in the Models Presented in Figures 3–6[a]

	Slab Dip Angle (deg)		Plate Size (km)	
	West	East	West	East
Figure 3	50	50	8,000	8,000
Figure 4	50	50	12,000	4,000
Figure 5	80	35	8,000	8,000
Figure 6	80	35	12,000	4,000

[a]East and west refer to the direction with respect to the mid-Pacific ridge while facing north.

which means that NR is nearly as fast as the average surface speed.

[18] The sign of γ indicates the direction of rotation: positive corresponds to a counterclockwise motion (similar to the present-day sense of NR), and vice versa. An alternative normalization can be performed using the average of the absolute no-net-rotation velocities instead of the average of the absolute velocities for the denominator of the ratio. This metric does not saturate for large NR, but it yields similar results than γ for our models. Therefore, for simplicity, we only discuss γ in the following.

3. Results

[19] We first analyze the effect of slab dip angle and ridge position on the net rotation and trench motions by discussing four representative models (see Table 2). We then discuss the role of slab viscosity, and that of the weak zones. The effect of changing the distribution of the asthenosphere from a continuous weak layer to one localized underneath oceanic regions is examined in section 3.4. In section 3.5, the influence of continental keels is analyzed for different asthenospheric distributions, keel depths, and the presence of upwellings. Lastly, we show that, in our models, γ is a function of plate size, slab dip angle, and slab viscosity.

3.1. The Role of Slab Dip and Ridge Position

[20] Figure 3 shows results for the most symmetric reference model. The asthenosphere is present underneath the oceanic plates only, and the slabs are as stiff as the lithosphere (Table 1). We show the dynamic pressure, which is the total pressure minus the lithostatic component, and the flow velocities.
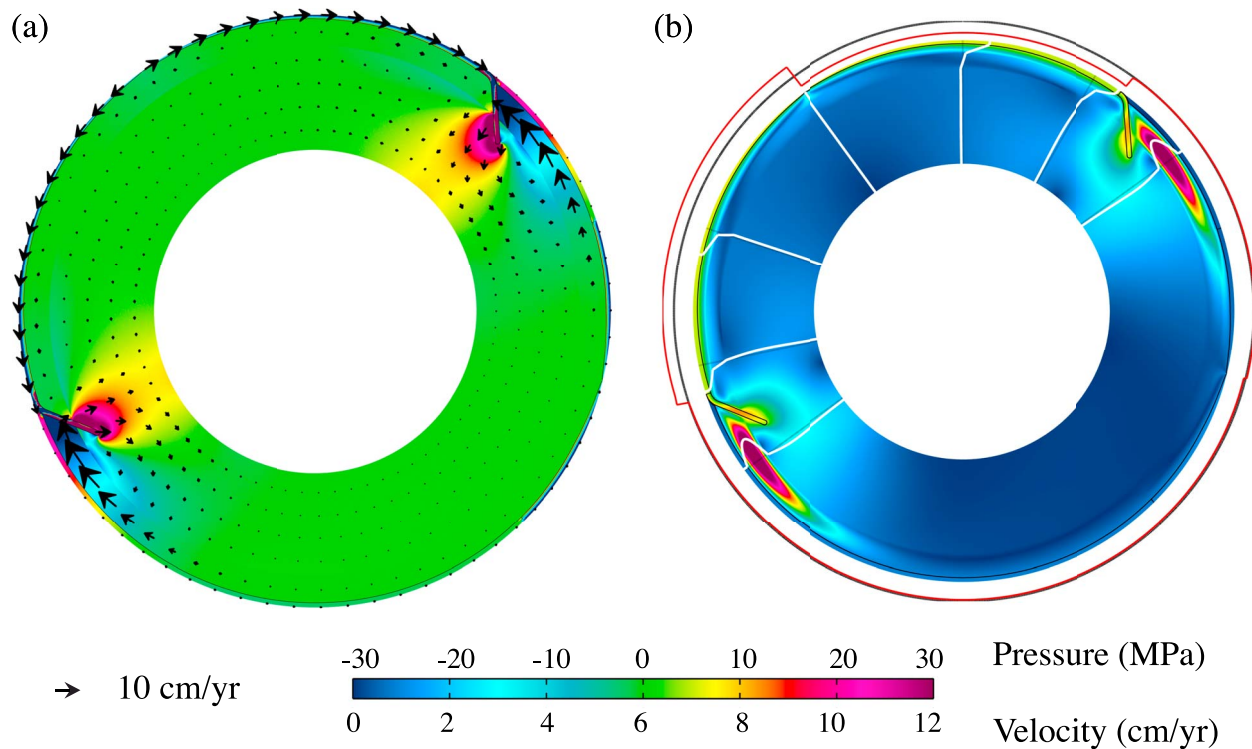
[21] NR is absent from a model that is purely symmetric in term of slab dips, distance between Pacific and Atlantic ridges, size of all plates, and has no additional LVVs. However, along the equator of the NR, Eurasia and South America have very different sizes, about as much as the size of the Pacific plate differs from the size of the Nazca plate (see Figure 1). Therefore, Pacific and Atlantic ridges are never diametrically opposed, which is illustrated in Figures 3–6 for two different Pacific ridge positions. Some NR is induced by the uneven distances on each side of the ridges ($|\gamma| \leq 0.1$). In the model represented in Figure 3, $\gamma = -0.08$. Besides the slight asymmetry between ridges, plates motions are symmetric on each side of the mid-Pacific ridge, and both trenches are stationary. We refer to the trench between the Pacific slab and Eurasia as the "Pacific trench", and the trench between the Nazca slab and South America as the "Nazca trench".

[22] Figure 4 illustrates the effect of changing the Pacific ridge position, similar here to the actual position in the Pacific basin, along the equator of NR. $\gamma = 0.45$ in this model. Such ridge asymmetry results in different slab thicknesses: 110 km for the Pacific plate and 82 km for Nazca, respectively, which explains the smaller dynamic pressure variations observed around Nazca. In Figure 4, asymmetric buoyancy forces result in asymmetric plate speeds: the speed of the smaller plate decreases, while that of the larger plate does not change significantly with respect to Figure 3. The Nazca trench retreats slowly, and the Pacific trench becomes nearly stationary.

[23] In order to isolate the effect of asymmetric buoyancy forces from that of ridge position, we ran a model with an asymmetric ridge position such as in Figure 4, symmetric slab dipping at 50°, and a seafloor that thickens up to its maximum depth in 10 My. This setup induces symmetric ridge push and slab pull forces. In such models, the Nazca and Pacific plates move at virtually identical speeds, trench motions are symmetric (no westward motion of the trenches), the dynamic pressure field is symmetric, and $\gamma = 0.36$. This suggests that ridge position has a purely geometric effect that affects net rotation through differences in plate size, but the ridge position, strictly speaking, has a minor effect on force balance. These models also suggest that the effect of basal tractions should be small because the Pacific plate, despite being 3 times longer than Nazca, moves at a similar speed.

[24] The model in Figure 5 is designed to test the effect of asymmetric slab dips; the ridge position is symmetric as in Figure 3 but the Pacific slab dips at
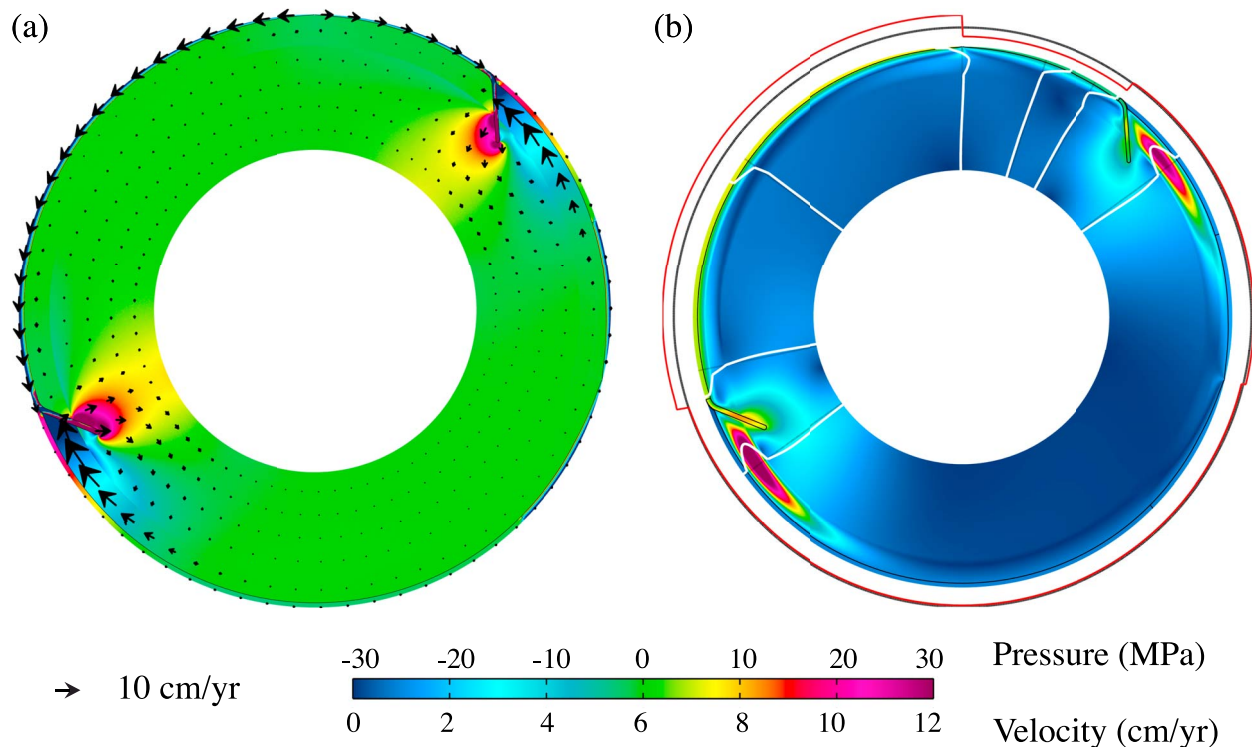
Figure 3. Reference model with a symmetric ridge position and symmetric slab dip angles equal to 50°. Both oceanic plates are 8,000 km long, and both slabs 110 km thick. (a) Dynamic pressure in MPa (colored background) and velocity vectors and (b) absolute velocities in cm/yr (colored background) and velocity profiles normalized by the maximum velocity of each profile. Profiles are shown at ridge, midplate, close to slab, and continental mantle wedge. The red line around Figure 3b shows the motions at the surface (amplitude and direction): A counterclockwise motion is plotted above the black line (the zero velocity) at a distance proportional to its velocity amplitude; likewise, a clockwise motion is plotted below. The color scale is saturated for both pressure and velocity. γ is equal to -0.08 and differs from zero because of the size difference between the South American and Eurasian plates. Both trenches are virtually stationary, and the flow profiles and dynamic pressures are symmetric on each side of the immobile mid-Pacific ridge. Fast return flow develops underneath the continental plates.

80° and the Nazca slab dips at 35°. Here, $\gamma = 0.45$, as in Figure 4, but the dynamics are very different. The nearly vertical slab pulls the western plate twice as fast as the shallow slab drives the eastern plate. Plate motions are strongly asymmetric, which promotes NR. The effective length of a slab that contributes to drive the plate is smaller for a flat slab than it is for a steep slab. This partially explains the difference in oceanic plate speeds. The dynamic pressures (Figure 5a) show two very different patterns: intense negative pressure develop above the shallow slab in the continental corner, while the oceanic corner experiences slight overpressures; around the steep slab, pressure in the oceanic and the continental corners are both negative. Mantle flow converges almost symmetrically toward the steep slab, while on both sides of the shallow slab, the flow tends to move toward the inside of the oceanic domain. The velocity profiles through the center of both oceanic plates indicate a

Couette style of mantle flow below the plates, which turns into a Poiseuille style of flow near both slabs. Mantle flow is westward beneath both oceanic plates near the slab hinge: faster than the oceanic plate on the steep slab side, and moving in the direction opposite to plate motion on the shallow slab side. Therefore, asymmetric slabs induce asymmetric mantle flow profiles in addition to asymmetric "effective" slab pull forces, which all tend to drive the plate with a steep slab faster than that with a shallow slab. Trench motions are westward in this model: slow advance of the Pacific trench, retreat of the Nazca trench. Slab return flow is much stronger toward the shallow dipping slab than toward the steep slab, but both overriding plates experience compression. The mid-Pacific ridge migrates toward the west at a fast speed (Figure 5b). Such ridge migration tends to reduce NR by decreasing the size of the fastest oceanic plate. This suggests that symmetric slab angles
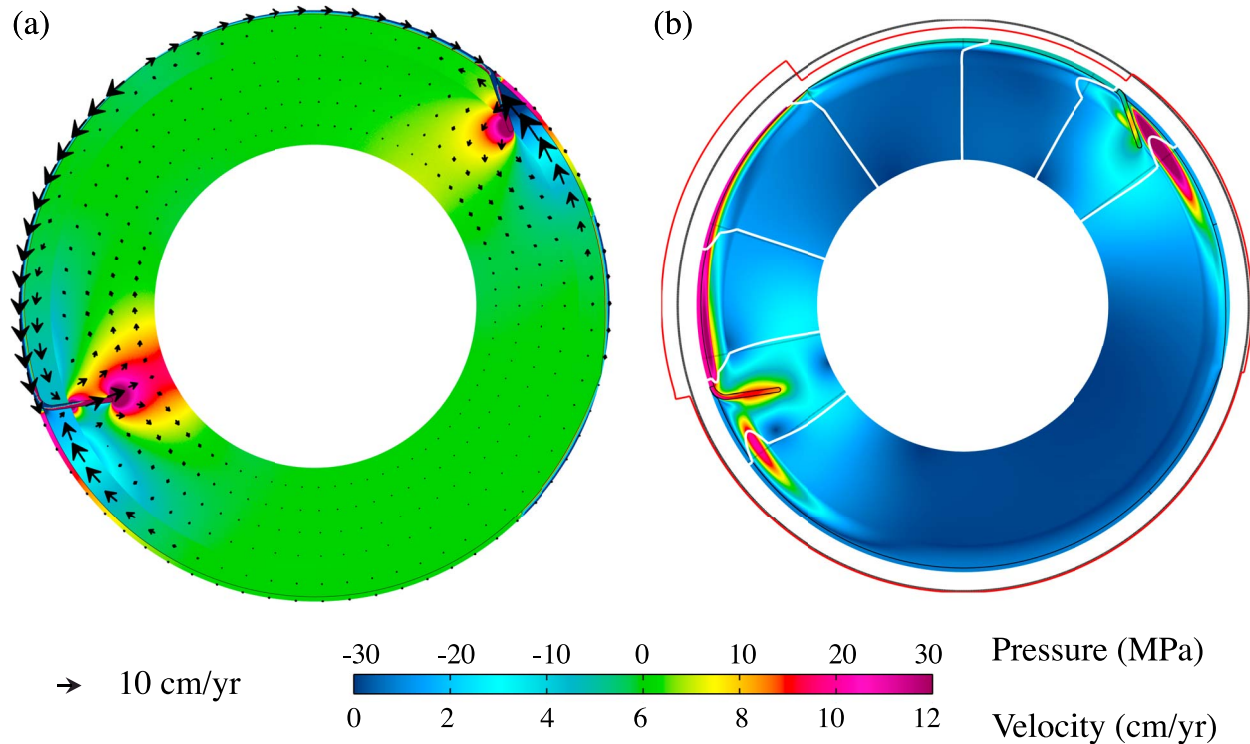
Figure 4. Model with an asymmetric ridge position and symmetric slab dip angles equal to 50°. (a) Dynamic pressure and velocity vectors and (b) absolute velocities and velocity profiles at depth and along the surface (see Figure 3). The position of the ridge corresponds to the actual location at present along the equator of the net rotation, ~12,000 km for the Pacific plate versus 4,000 km for the Nazca plate. γ is equal to 0.45; the Nazca trench retreats while the Pacific trench is stationary. Plates move at different speeds on each side of the ridge that migrates toward the fastest plate more rapidly than the trench retreats, which tends to reduce plate asymmetry.

induce a NR that can only be balanced by asymmetric plate sizes, potentially created through ridge migration.

[25] We Last combine both ridge and slab asymmetry in an end-member model that resembles the present-day Pacific domain (Figure 6). This model mimics most closely the plate and slab geometries along the equator of the observed NR. The resulting NR is $\gamma = 0.8$, that is, about as large as in HS-3, implying that the present-day Pacific basin setting may indeed induce large NR when measured in a Pacific hot spot reference frame. The flow profiles indicate that below Nazca, moving eastward, the mantle flows westward. In fact, in this model, the upper mantle flows westward beneath the entire Pacific basin (Figure 6b). Trench motions are westward (advancing Pacific trench and retreating Nazca trench), as seen for several reference frames [e.g., *Funiciello et al.*, 2008], and the ridge migration is faster than in Figure 5. Trench advance is slower than trench retreat, compatible with the ongoing closure of the Pacific domain. The pressure solution (Figure 6a) is dominated by the effect

of slab dip asymmetry over that induced by asymmetric slab buoyancy (resulting from an asymmetric ridge position).

[26] Ridge and slab asymmetry both induce significant NR. Our models suggest that trench motions are primarily controlled by slab dip angles when the slabs are stiff. A realistic asymmetric ridge position in the Pacific does not yield westward trench motions on its own [*Nagel et al.*, 2008]. On the one hand, Figures 3–6 show that asymmetric slab dips result in different pressure fields around the slabs, which means that the dynamics differ (compatible with analytical corner flow solutions, [e.g., *Tovish and Schubert*, 1978; *McKenzie*, 1979]). On the other hand, ridge asymmetry mostly has a geometric effect (uneven plate sizes) that alters the average surface velocity but not the main driving forces. This is further discussed below. The flow profiles in Figure 3–6 show that a shear-driven flow develops below the oceanic plates, in the asthenosphere, away from the slabs. Closer to the slab hinge, this Couette style of flow turns into a Poiseuille style of flow, where the underlying asthenosphere moves

Figure 5. Model with a symmetric ridge position and asymmetric slab dips equal to 80° on the western side (Pacific plate) and 35° on the eastern side (Nazca plate). (a) Dynamic pressure and velocity vectors and (b) absolute velocities and velocity profiles at depth and along the surface (see Figure 3). $\gamma = 0.45$, similar to that in the model shown in Figure 4. A stronger effective slab pull is exerted by the steep slab, and plate motions are strongly asymmetric. The pressures in the upper mantle show two very different patterns: intense negative pressures occur above the shallow slab, in the continental slab corner, while the oceanic corner experiences slight overpressures; around the steep slab, pressures in the oceanic and the continental corners differ only slightly, both being negative. Trench motions are westward (advance of the Pacific trench, retreat of the Nazca trench), and slab return flow is stronger toward the shallow dipping slab.
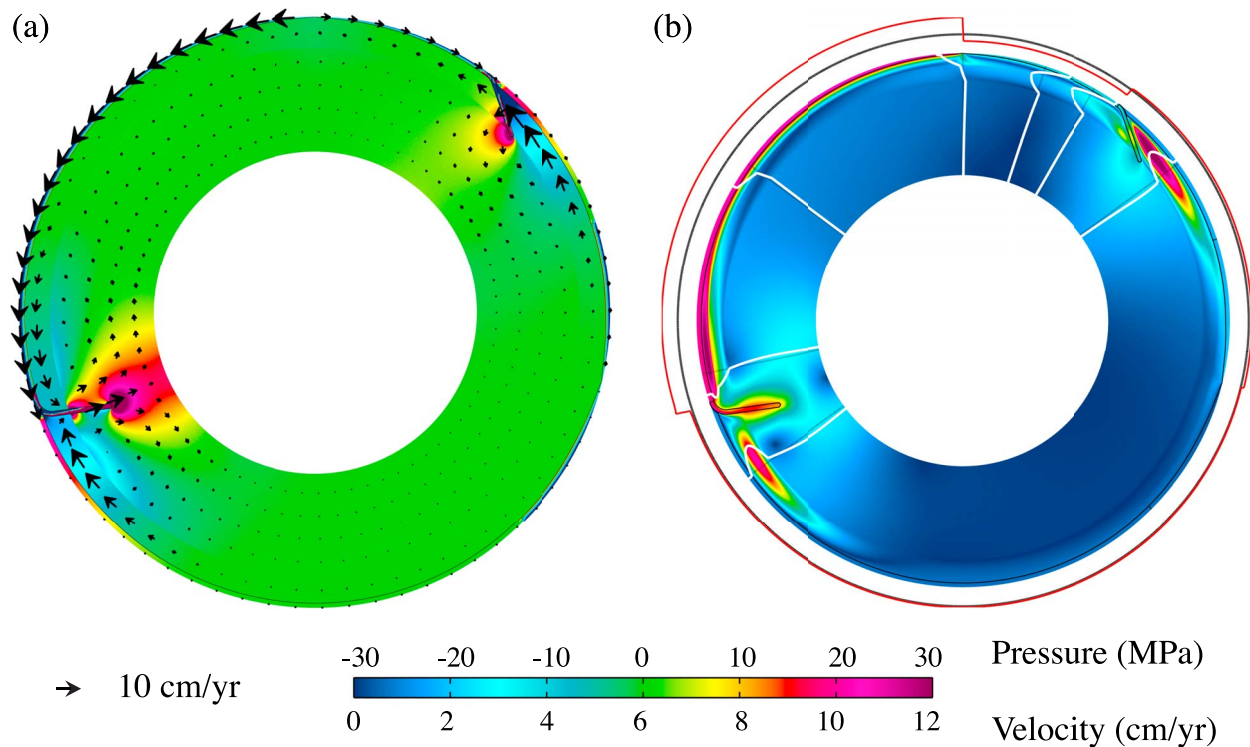
faster than the plates [cf. *Hoink and Lenardic*, 2008, 2010; *Becker and Kawakatsu*, 2011; *Billen and Jadamec*, 2012].

[27] We ran models similar to those in Figures 3–6 while varying slab dip angles from 35° to 50°, 65°, and 80° for each of the Pacific and the Nazca slabs, and using several ridge asymmetric positions. We found that in all models, the oceanic ridge migrates so that it reduces NR. Models with an asymmetric ridge position indicate that the ridge moves toward the center of the oceanic basin at a faster speed than the Nazca trench retreats, which reduces plate size asymmetry. In these models, the speed of ridge migration toward the center of the basin increases with plate and slab dip asymmetry. This only holds for a Nazca plate length that is larger by at least a factor 2 than the length of the slab (1200 km). When the plate is too small, any slab dip angles steeper than 50° cause the ridge to move toward the subduction zone and the trench to retreat, which can

eventually result in the disappearance of the small plate. In models with a symmetric ridge position, asymmetric slab dip angles also cause the ridge to migrate toward the faster plate, as illustrated in Figure 5. The present-day net rotation could be peculiar to the configuration of the Pacific domain, and perhaps result from transient, regional slab dynamics [e.g., *Zhong and Gurnis*, 1995; *Di Giuseppe et al.*, 2009; *Faccenna et al.*, 2009].

[28] These models were also ran using a weaker mantle wedge above each slab. The results differ mostly in term of local dynamics, but not significantly in terms of NR. When the slab retreats, a weak mantle wedge is more rapidly sucked into the slab corner; however when the slab advances, a weak wedge is less entrained in the slab corner than a strong wedge.

[29] All models suggests that trench motions significantly modify the behaviors expected from kinematic corner flow solutions.

Figure 6. Model with an asymmetric ridge position, same as in Figure 4, and asymmetric slab dip angles equal to 80° on the western side (Pacific plate) and 35° on the eastern side (Nazca plate). The geometry of the plates and slabs in this end-member model resembles the actual plate geometry along the equator of the net rotation. (a) Dynamic pressure and velocity vectors and (b) absolute velocities and velocity profiles at depth and along the surface (see Figure 3). γ = 0.8, similar to HS-3. Small differences in the dynamic pressures arise compared to Figure 5 from the addition of an asymmetric ridge location. However, this asymmetry creates a large plate that goes fast as a result of steep slab angle and a small plate that goes slow as a result of shallow slab angle. This configuration promotes large NR amplitudes.
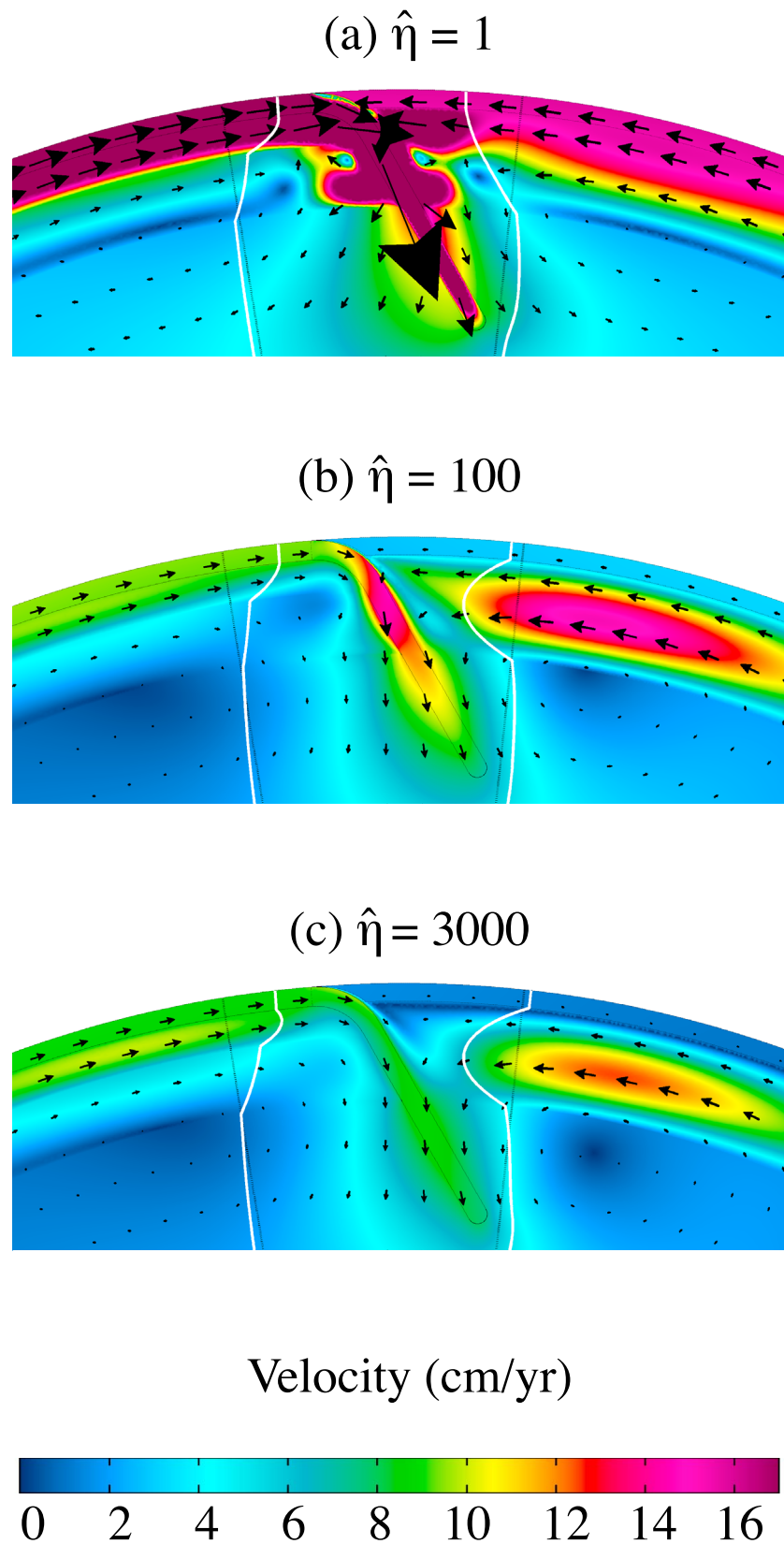
3.2. The Role of Slab Viscosity

[30] In this section, we examine the changes that arise from varying slab viscosity while maintaining lithospheric viscosity constant. We focus on one example (Figure 7) where only the eastern slab dipping at 65° is shown. This particular model has a symmetric ridge position and a western slab dipping at 80° so that the amount of net rotation remains small, less than 0.1, and only affects the results moderately.

[31] The velocity profiles, a combination of Couette and Poiseuille flow, indicate that, as the slab stiffens from upper mantle to lithospheric viscosity, a return flow develops underneath the overriding plate. The return flow becomes gradually faster as slab stiffness increases. The case in Figure 7a is an end-member in which the slabs are as weak as the upper mantle. There, surface plate velocities are faster than mantle flow. The case in Figure 7b represents intermediate slab viscosity, and shows that a rapid flow develops in the upper mantle, beneath the continental overriding plate. In the case
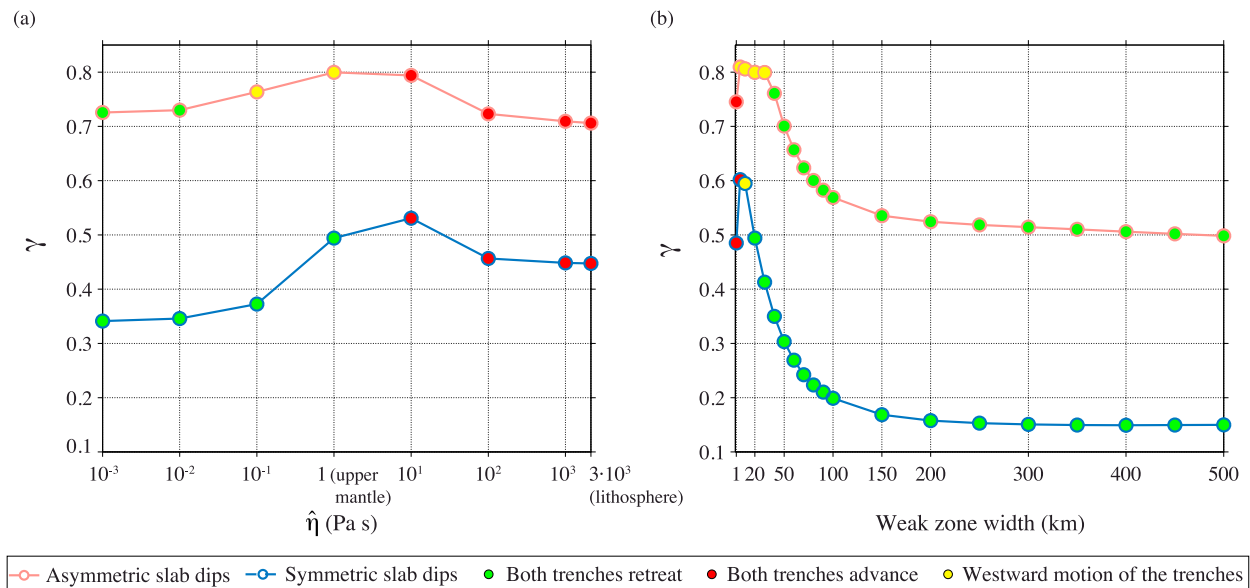
in Figure 7c, the slabs are as stiff as the plates, that is, 3,000 times stiffer than the upper mantle. In this case, the amplitude difference between plate speed and return flow is the largest of all models considered, although the trench is slowly advancing in the direction opposite to that of the return flow. There is an anticorrelation between the speed of the overriding plate, and the amplitude of the velocity contrast between that plate and the return flow: the slower the overriding plate, the larger the velocity contrast, and vice versa. Our models suggest that the fast slab return flow below the overriding plate arises from (1) relatively stiff slabs; (2) a strong viscosity contrast between the plates and the underlying upper mantle, which in our model is within the range discussed by *Hoink and Lenardic* [2008, 2010], *Becker and Kawakatsu* [2011], and *Billen and Jadamec* [2012]; and (3) slab dip angles (see Figures 5 and 6), which induce a faster return flow for shallow slab dips.

[32] This example also illustrates the role of slab viscosity in driving the net rotation. Weaker slabs

(a) $\hat{\eta} = 1$

(b) $\hat{\eta} = 100$

(c) $\hat{\eta} = 3000$

Velocity (cm/yr)

0   2   4   6   8   10   12   14   16

Figure 7. Velocity field (arrows), absolute velocities (in cm/yr, colored background), and normalized velocity profiles (white vertical curves) for three different cases of slab viscosity contrast $\hat{\eta}$, defined as the ratio of slab over upper mantle viscosity. Pressure-driven flow forms in the asthenosphere that is present underneath the oceanic plates only.

Figure 8. Net rotation as a function of (a) the viscosity ratio $\hat{\eta}$ and (b) the thickness of the weak zones at the trench. The blue and pink curves refer to the models shown in Figures 4 and 6, respectively. Yellow dots indicate that a westward motion of both trenches occurs, while green dots indicate that both trenches retreat and red dots indicate that both trenches advance.

sink faster, and tend to drive symmetric plate motions around them (see Figure 7a). Symmetric plate motions toward the slab and rapid trench retreat are characteristic of a lithospheric drip or "slab suction" type of driving mechanism. Such a mechanism, when both subducting and overriding plates have similar velocities and sizes, must generate very small net rotations. On the contrary, stiff slabs are good stress guides that transmit "slab pull" efficiently and drive the subducting plate faster than the overriding plate, and promote trench advance [*Conrad and Lithgow-Bertelloni*, 2002] as shown in Figure 7c (see flow profile showing trench advance). Therefore, weak slabs naturally induce small net rotation whereas strong slabs largely promote the net rotation. This is in agreement with the argument that LVVs induce NR. These consequences of plate strength on trench motions have also been observed experimentally [e.g., *Faccenna et al.*, 2007; *Schellart*, 2008] and numerically [e.g., *Enns et al.*, 2005; *Di Giuseppe et al.*, 2008; *Stegman et al.*, 2010].

3.3. The Role of Weak Zones

[33] The degrees of coupling between adjacent plates might play a major role in the net rotation of the lithosphere, and this is intimately related to the numerical treatment of the weak zones (WZ). While we kept the properties of the WZ constant in the models shown in the previous sections (cf. Table 1),

we suggest here that these properties may exert a significant control on γ. We explored the role of the WZ at the trench, focusing on their thickness and viscosity.

[34] We found that, at a constant WZ thickness of 20 km, the viscosity ratio of the WZ over the upper mantle ($\hat{\eta}_{wz}$) should be less than 10 in order for the trenches to show both advancing and retreating behavior (Figure 8a). While the largest $\hat{\eta}_{wz}$ consistently result in trench advance for all slab dip angles, the lowest $\hat{\eta}_{wz}$ consistently induce trench retreat. Both the largest and lowest $\hat{\eta}_{wz}$ that we used yield lower NR: γ decreases by up to 0.1 for $\hat{\eta}_{wz} = 3 \cdot 10^3$, the same stiffness as the plates, and γ decreases by up to 0.25 for $\hat{\eta}_{wz} = 10^{-3}$.

[35] Figure 8b shows the variations in γ obtained for different WZ thicknesses. The amplitude variations in γ are larger than those observed as a function of $\hat{\eta}_{wz}$. A rapid decrease in γ occurs with an increase in WZ thickness, which levels off at a value of ~2° (~220 km). This has important implications for the maximum amplitude of the net rotation that can be generated in numerical models. *Zhong* [2001], for instance, used 400 km wide (i.e., ~4°) plate margins.

[36] Figures 8a and 8b indicate that weak zone strength and width do not have an opposite and interchangeable effect. These results suggest that fine local resolution may be required to accurately

model global patterns of plate motions [*Stadler et al.*, 2010]. Figure 8 also shows that reaching the maximum γ requires a larger coupling (i.e., stiffer, or thinner WZ) for symmetric slabs dipping at a 50° angle than for asymmetric slab dips. Indeed, models with symmetric dips reach the largest γ for WZ that are either one order of magnitude stiffer, or 20 km thinner than the models with asymmetric slab dips. The length of the WZ cannot explain this effect, because at the radius of curvature that we are using (300 km), slabs have a nearly constant surface area in contact with the overriding plate (∼260 km) regardless of slab dip angle. However, steep slabs appear to be more coupled with the overriding plate, as they are the most likely to yield trench advance. Following the argument of *Di Giuseppe et al.* [2008], we suggest that, because steep slabs are harder to unbend at the hinge than shallow ones, they are more directly coupled with the upper plate. Therefore, models that include at least one steep slab reach a maximum coupling threshold at lesser WZ strength and width than a model with flatter slabs.

[37] Figure 8 and other tests for different slab dip angles (not shown) indicate that the width of the weak zones controls the amplitude of γ to a fairly similar extent for multiple combinations of slab dip angles and ridge asymmetry. We therefore argue that the slabs and ridge effects that we identify hold for a broad range of WZ widths, provided that the weak zone properties are maintained identical between all models.

3.4. The Role of the Asthenosphere

[38] In this section, we estimate how our assumption that the asthenosphere exists mainly underneath the oceanic plates affects our results. We extend this low-viscosity layer underneath all plates, between their base and 300 km depth. This asthenosphere remains one order of magnitude weaker than the upper mantle viscosity, as in sections 3.1 and 3.2. The slabs are as stiff as the plates, similar to the reference models shown in 3.1, and we vary slabs dips as described above. When the asthenosphere is present underneath all plates, the slabs constitute the only LVVs between the base of the plate and 300 km depth.

[39] We found that a global asthenosphere changes upper plate and trench motions significantly. The model in Figure 9 is similar to that in Figure 6 with the asthenosphere present beneath all plates. Here, $\gamma = 0.78$, roughly similar to that in Figure 6. A global asthenosphere results in a faster advance

of the Pacific trench and westward motion of Eurasia (∼3 times faster), and a slower retreat of the Nazca trench and South America (∼ half slower). Therefore, an underlying asthenosphere does not consistently result in faster continental motions. The Nazca plate is ∼ twice as fast and the Pacific plate ∼1/3 faster. Faster slab velocities result from a weaker mantle and less resistance from of the overriding plate, which is more free to move.

[40] Strong subducting slabs promote trench advance [e.g., *Conrad and Lithgow-Bertelloni*, 2002], even more so in models with a global asthenosphere. We suggest that this arises from a reduced coupling between plates and mantle, thereby emphasizing the coupling between adjacent plates. Figure 9a shows that a ubiquitous asthenosphere significantly reduces pressure in continental plates with respect to Figure 6a, despite the broader and faster return flow that develops. This suggests that the asthenosphere introduces a decoupling that has a stronger role than the mantle return flow in controlling trench motions. Furthermore, we advocate that a certain degree of coupling between overriding plate and underlying mantle is necessary in order to yield trench retreat and overcome the lateral pressure exerted by strong subducting slabs.
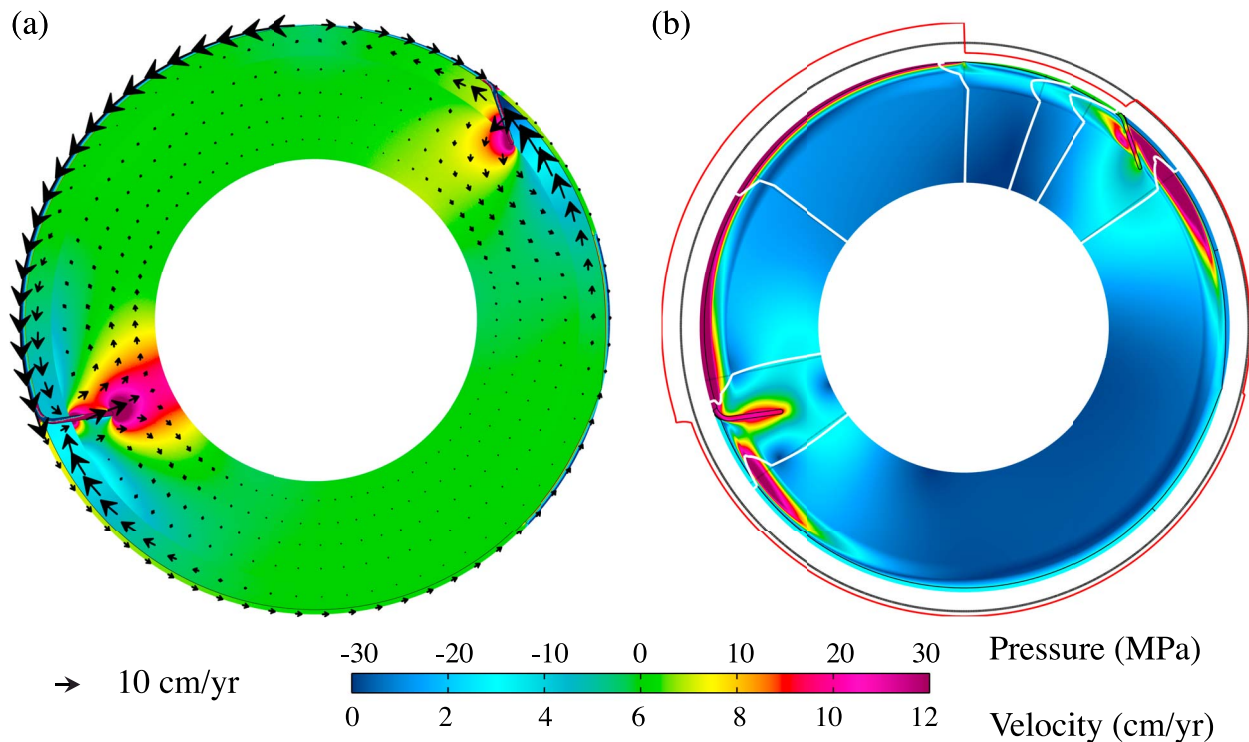
[41] Overall, a global asthenosphere results in faster oceanic to continental plate speed ratios, which supports the findings of *Becker* [2006]. Trench advance is also less likely than trench retreat at present. Thus, we argue that a weaker mantle confined underneath the oceanic plates is more plausible.

3.5. The Role of Continental Keels and Upwellings

[42] We next explore the role of continental keels (Figure 10) for different keel thicknesses, widths, and locations. We also consider their effect in the presence of two schematic upwellings below the western Pacific plate and western Africa/Eurasia, or the presence of an asthenosphere beneath continental regions.

[43] The width and location of the keels have an effect on the pressure in the continental arc corner [*O'Driscoll et al.*, 2009], but we found that these two keel properties have a minor effect on γ and trench motions. For this reason, we only show the results of models where the width of the keels was fixed: 6,000 km underneath Eurasia and 2,000 km underneath South America. Cratonic keels in both Eurasia and South America do not stand close to
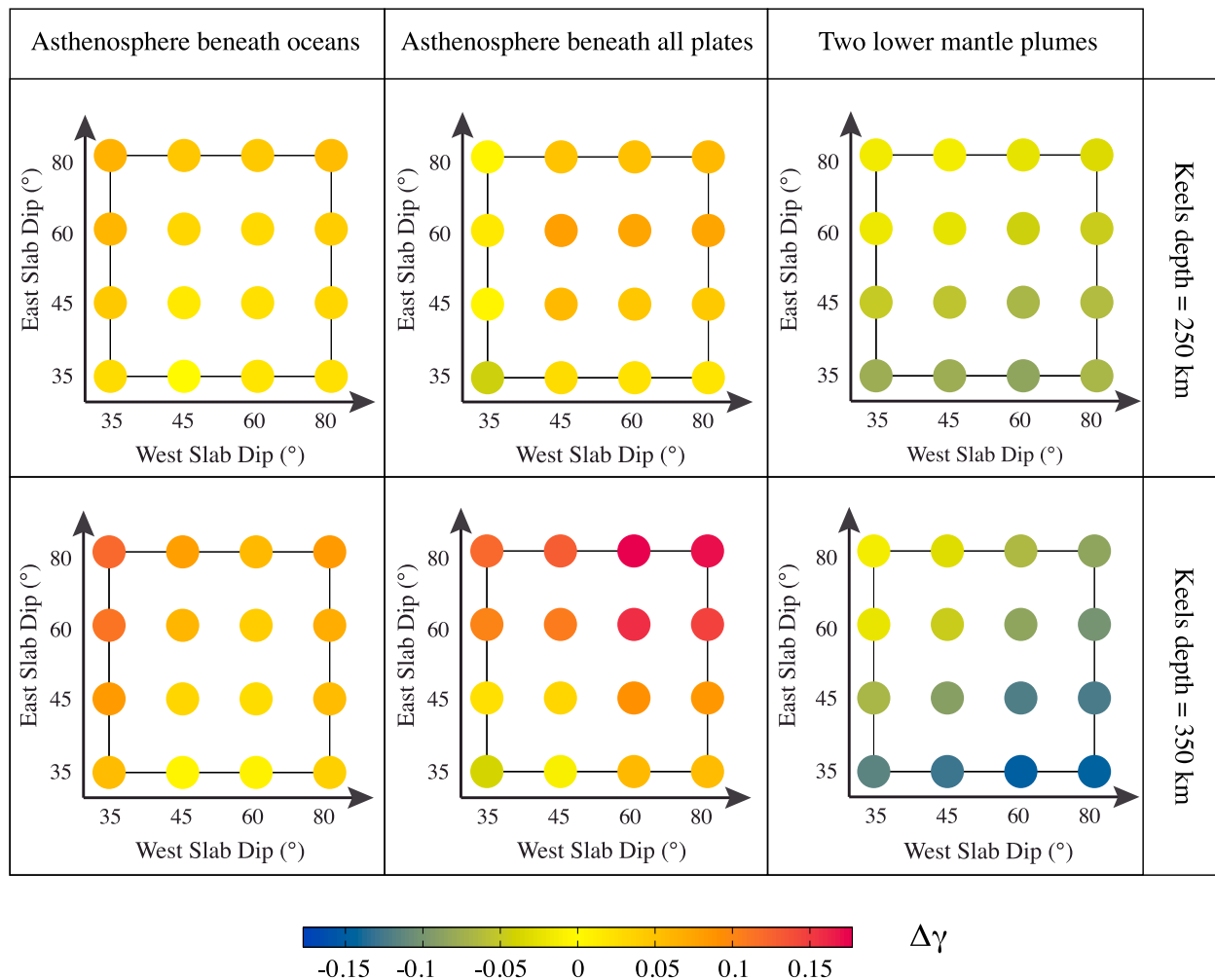
(a)

(b)

-30   -20   -10   0   10   20   30   Pressure (MPa)

➔   10 cm/yr

0   2   4   6   8   10   12   Velocity (cm/yr)

Figure 9. Model with asymmetric ridge position and slab dips (80° for the Pacific slab and 35° for the Nazca slab). The model differs from that in Figure 6 by the presence of an asthenosphere underneath all plates. (a) Dynamic pressure and velocity vectors and (b) absolute velocities and velocity profiles at depth and along the surface (see Figure 3). $\gamma = 0.78$. Despite stronger return flow, slower trench retreat (Nazca), and faster trench advance (Pacific), the pressure increase in the upper plates toward the slab is significantly smaller than in the model shown in Figure 6b.

the subduction zones along the equator of the net rotation, so we fixed the distance between the keel and the subduction zone to 3,000 km for Eurasia, and 1500 km for South America. In our models, the pressure increases by up to half an order of magnitude in the slab corner from the presence of a nearby keel, with respect to a model with no keel (in agreement with *O'Driscoll et al.* [2009]). The effect of the keels and the distribution of the asthenosphere are not directly opposed, although both affect the amplitude of NR to a small extent. With the addition of a keel, models where the asthenosphere is present underneath all plates show a minor pressure increase in the continent toward the trench (cf. Figure 9). The absence of an asthenosphere underneath the continents results in a continuous pressure increase from the passive margin toward the trench (e.g., Figure 6), while adding a keel always confines the pressure increase between the edge of the keel and the trench. Continental deformation is expected to be significantly different between these two cases.

[44] Figure 10 summarizes the effect of continental keels on net rotation. We show a difference in γ,

$\Delta\gamma$, that is computed with respect to an identical model with no keel, called "reference model". For the first column, the reference models are those that have been discussed in section 3.1. For the second column, the reference models are those discussed in the previous section on the effect of asthenospheric distribution. Last, the reference models with two upwellings and no keels used in the third column are not discussed separately.

[45] We find, first, that deeply anchored continental keels (350 km deep) affect the amplitude of γ twice as much as shallow keels (250 km deep). Secondly, the variations in γ that result from adding continental keels are significantly less pronounced than those observed for different ridge positions, and slab dip angles and viscosities (each up to $\Delta\gamma = 0.6$). Thirdly, the keels have a stronger influence in models where the asthenosphere extends laterally underneath the continental regions. This is due to the larger viscosity contrast between the keels and the material underneath the plates, which results in stronger LVVs; it is also due to the faster and broader slab return flow that develops within the upper mantle when there is an asthenosphere,

Figure 10. $\Delta\gamma$ is the difference in net rotation obtained between two models that differ only by the presence or absence of continental keels. The effect of continental keels is twice as large when the keels extend to 350 km than 250 km. A weak asthenosphere defined underneath all plates (second column) tends to increase the net rotation induced by the keels, while the upwellings (third column) tend to reduce it. Nonetheless, the effect of keels in a model with upwellings depends on their relative positions and dimensions.

which tends to entrain the keel (and the plate above) toward the slab at a faster rate. Continental keels (with or without an asthenosphere underneath them) have a tendency to moderately increase the amplitude of the net rotation in models without upwellings. However, idealized upwellings tends to push keels away from themselves, in a way that may increase or decrease γ. Note that the addition of upwellings changes the total amount of energy available to drive the system. Whether keels result in larger or smaller γ depends on their location with respect to the upwellings: if the net rotation is counterclockwise, an upwelling to the east of a keel yields faster γ, while an upwelling to the west of a keel yields slower γ. Figure 10 (third column) shows that keels decrease γ in such models, and do

so to a larger extent for steep western slab dips and shallow eastern slab dips. This decrease is mainly due to the eastward push that the swell underneath Africa exerts on the keel below Eurasia. For this reason, keels have more impact in the models that make the trench in Eurasia advance (those having the aforementioned strong slab dip asymmetries), because the eastward push from the upwelling makes the Pacific trench retreat, which decreases γ. The keel underneath South America is too far from the two major upwellings to have a significant effect. The flow generated by the upwelling in the western Pacific is mostly confined to the Pacific oceanic domain, and therefore does not interact much with the keel underneath Eurasia.

[46] These results suggest that keels can influence the net rotation to a relatively small extent, and mostly when they extend below asthenospheric level and interact with strong slab return flow or with an upwelling. This is in agreement with the results of *Gurnis and Torsvik* [1994], *O'Driscoll et al.* [2009], and *van Summeren et al.* [2012] on the influence of keels on plate motions. *Zhong* [2001] and *Becker* [2006] found that continental keels can generate small amounts of NR, within a similar range to that indicated by our results.

3.6. Net Rotation as a Function of Plate Size, Slab Dip Angle, and Slab Viscosity

[47] Our results suggest that the parameters that exert the strongest controls on γ are the viscosity contrast between slabs and upper mantle ($\hat{\eta}$), the size of the oceanic plates that enter subduction zones, and the slab dip angles. Other parameters such as the position of the Atlantic with respect to the Pacific ridge, the continental keels, and the asthenosphere distribution play less of a role, although they all have some effect. We now show that we can express γ based on a relationship that combines the most important variables in our study. The velocity of the two oceanic plates dominate the velocity average at the surface, which is a primary control on γ. These two plates are the idealized Nazca and Pacific plates, and we have observed that the dip angle of the slab attached is the most significant variable in controlling their speed. We suggest that the "effective" slab pull force depends not only the mass anomaly from the slab but also on its orientation with respect to the vertical axis, and therefore slab dip angle. The results shown in section 3.2 indicate that the amplitude of γ is also dependent on the viscosity of the subducting slabs. Therefore, we combine these variables into the following expression:

$$\gamma = P(\log(\hat{\eta}), \delta_W, \delta_E, L_W, L_E)$$
$$= (S \log(\hat{\eta}) + C) \frac{L_W \sin(\delta_W) - L_E \sin(\delta_E)}{L_W + L_E} \quad (1)$$

where we have used the indices E and W for the eastern (Nazca) and western (Pacific) slabs and plates, L is the length of an oceanic plate, and δ is the slab dip angle of a slab. P is a nondimensional parameter. $S \log(\hat{\eta}) + C$ is the linear relationship that links γ to the natural logarithm of slab viscosity. The arbitrary constants S and C have different values for models with symmetric ($S = 0.45$ and $C = -1.18$) and asymmetric ridge positions ($S = 0.37$ and $C = -1.03$). This relationship is defined
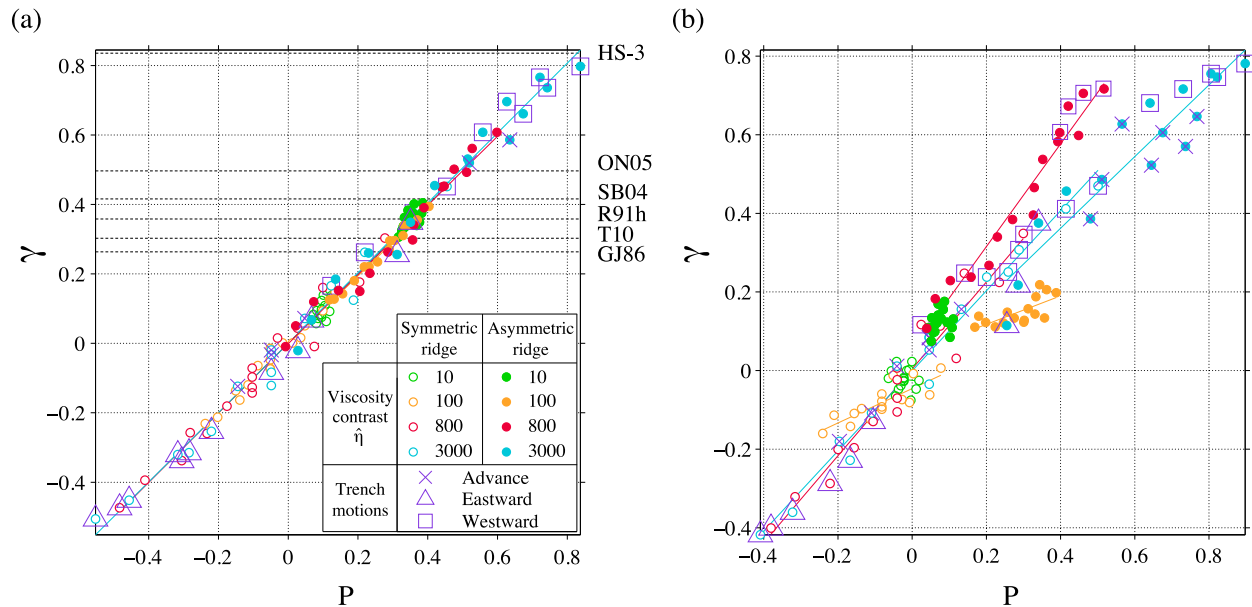
for the normalized measure of net rotation that we are using. The plate velocities themselves depend upon the density contrast between the slabs and the mantle, and the viscosities. γ is expected to saturate for large slab viscosity contrasts (larger than those we have tested here and not realistic for the present-day Earth).

[48] γ does not follow the logarithmic dependence on slab viscosity when slabs are as weak as the upper mantle ($\log(\hat{\eta}) = 0$), and cannot be represented using equation (1). γ can nonetheless be plotted on a single line using the relationship $(L_W \sin(\delta_W) - L_E \sin(\delta_E))/L_W + L_E$ which gives a slope of -0.09 for a symmetric ridge position, and -0.17 for an asymmetric ridge position.

[49] The net rotation amplitudes computed in all 256 models are plotted as a function of P in Figure 11. Figures 11a and 11b show the results of models where the asthenosphere is present underneath the oceanic plates only, and underneath all plates, respectively. Two cases of ridge asymmetry are represented: a symmetric ridge position (open symbols), and an asymmetric ridge position (filled symbols) corresponding to the position of the EPR along the equator of the net rotation. We show the results from models with slab dip angles of 35°, 50°, 65°, and 80° for each of the western and the eastern slabs.

[50] Figure 11a shows that equation (1) holds for a wide range of slab viscosity contrasts in models where the asthenosphere is localized underneath oceanic regions. Equation (1) is simple because it contains information about the oceanic plates only. As discussed in section 3.4, a global asthenosphere results in faster continental motions, which are not accounted for in equation (1). Therefore, P is able to capture the important variables that control γ in models where the mantle is weaker below the oceanic plates, but lacks information about continental velocities in order to fully portray γ in the models shown in Figure 11b. These models indicate that ∼ half of the models with stiff slabs ($\hat{\eta} = 3,000$) result in trench advance simultaneously at all subduction zones. This is unlike Earth based on trench motion compilations [*Heuret and Lallemand*, 2005]. Weaker slabs result mostly in trench retreat, although $\hat{\eta} = 800$ presents a few cases of westward trench motions, all corresponding to the faster predicted γ for that viscosity contrast. These results, along with those of section 3.4, tend to favor the cases where a weaker mantle is localized underneath oceanic regions. If this is the case, our analysis suggests that a simple relationship exists between γ and

Figure 11. Net rotation amplitudes and trench motions from 256 numerical simulations using variable slab dip angles and viscosities, and two different ridge positions (symmetric, as in Figures 3 and 5, or asymmetric, as in Figures 4 and 6). (a) Models where the asthenosphere is present underneath the oceanic plates only and (b) models where the asthenosphere is present underneath all plates. See text for the derivation of the nondimensional parameter P. Most trenches retreat, so we only highlight the models that show trench advance (crosses) and a single direction of motion: toward the west (squares) and toward the east (triangles). The curves show linear fits to the data for each slab viscosity contrast and each ridge position. The black dashed lines and labels in Figure 11a show the net rotation amplitudes contained in the kinematic models shown in Figure 1 using our normalized measure of the net rotation.

plate size, slab strength, and effective slab pull. The asymmetric ridge position results in an offset of the results toward larger net rotations, while the dependence on P remains very similar. The slopes of the fits to the modeling results is unity for the symmetric ridge cases, and the intercept zero. Small variations exists for the cases with an asymmetric ridge position (slopes variations from 0.92 for the weakest slabs to 1.01 for the strongest slabs). The maximum net rotation that can be induced depends strongly on slab strength [cf. *Piromallo et al.*, 2006]. The range of amplitude variations of γ is only ∼0.15 for a slab viscosity contrast of 10, while it is ∼0.8 for a viscosity contrast of 3,000.

[51] Trench retreat is typical for the models shown in Figure 11. A more unusual setting is when both trenches advance, or move eastward or westward. Those are highlighted by different symbols in Figure 11. We find that it is possible to obtain a unidirectional motion of the trenches by combining, firstly, stiff slabs (viscosity contrasts of 800 or 3,000), and secondly, asymmetric slab dip angles. The ridge position does not seem to play a major role, because a unidirectional motion of the trenches occur in models where the ridge is symmetric as well as in models where it is asymmetric. Steep, stiff slabs tend to result in trench advance, while shallow slabs result in trench retreat. Weaker slabs consistently show trench retreat (Figures 11a and 11b). The same conclusions were reached by *Faccenna et al.* [2007] using analog experiments, and the correlation between slab dip angle and trench behavior has also been observed in nature [*Lallemand et al.*, 2005].

[52] The ridge position does not seem to affect this general behavior. Our analysis shows the consequences of asymmetric ridge push (or gravitational sliding) on the amplitude of γ to be minor, as well as the consequences of asymmetric slab thicknesses, which differ by 28 km. None of these effects are accounted for in equation (1), as they do not improve the correlation. This can also be deduced from Figure 4 where the difference in plate velocities on each side of the Pacific spreading center are relatively small. We also ran models with neutrally buoyant slabs to isolate the effect of ridge position as discussed by *Nagel et al.* [2008]: the resulting plate velocities are always smaller by at least one order of magnitude than when slabs are included. It is likely that this contribution results in

the modest variability observed in the slopes in Figure 11a for an asymmetric ridge position.

4. Discussion

[53] Our study is focused on the Pacific domain that is bound by subducting slabs, mostly distant from slab windows near the equator of the net rotation. This flow system may represent a roughly cylindrical structure at a global scale [*Husson et al.*, 2008]. We therefore expect the addition of a third dimension to modulate the amplitude of the net rotation and extend the variety of system behaviors, but not to render the processes that we identified ineffective. Our end-member, simplified models should provide valuable information on the first order dynamics in the Pacific setting, and the geological features that control NR. While 3-D spherical convection models result in the most realistic setups, they make it numerically more challenging in term of computational cost and practical implementation to study a wide range of parameters in a systematic manner. In our models, the mantle flow restricted to 2-D is likely to emphasize NR. Among all the harmonic degrees of toroidal flow that LVVs may generate, only a net shear between the bottom and the surface of the model can develop. For instance, the effects of slab width and toroidal flow around the edges of slabs [e.g., *Funiciello et al.*, 2003, 2004; *Piromallo et al.*, 2006; *Royden and Husson*, 2006; *Schellart et al.*, 2007] are absent from our models.

[54] This study does not constrain the amplitude of the net rotation on the present-day Earth. Our models indicate instead that a broad range of net rotation amplitudes can be generated in different configurations encountered in the Pacific domain, including values as high as those contained in HS-3. A rigorous evaluation of the present-day NR requires high-resolution 3-D modeling that accurately represents the great variety of ridge positions and slab geometries found globally and in the Pacific domain, as well as a better knowledge of slab and asthenospheric rheology.

[55] *Ricard et al.* [1991] and *Zhong* [2001] suggested that present-day NR results from the velocity contrast between fast oceanic plates and slow continental plates, which they explained based on the existence of continental keels and the possible absence of asthenosphere underneath continents [*Zhong*, 2001; *Becker*, 2006]. We argue that the forces acting on oceanic plates are more likely to be responsible for present-day NR than the forces acting on continental plates, in particular when the asthenosphere is restricted to suboceanic plate domains. We found that two principal geologic features can induce significant NR: stiff slabs with steep versus shallow dip angles on opposite sides of the Pacific oceanic basin along the equator of NR, and a ridge that is located away from the center of the Pacific. The slabs are the main active sources of NR in this study [cf. *Faccenna et al.*, 2007, 2009].

[56] The effects of an asymmetric ridge position in the Pacific have been discussed by *Nagel et al.* [2008] in relation to the current westward Pacific trench motions observed in several absolute reference frames. The driving forces in their models come from pressure gradients underneath the lithosphere, which are related to the ridge position. *Nagel et al.* [2008] concluded that the ratio of the size of the Nazca plate over that of the Pacific plate should be equal to 1/10 or less in order to obtain westward trench motions. However, the sizes of the Nazca and Pacific plates at present are such that this ratio is equal to ~1/3 or more. Therefore, the asymmetry of the EPR is not large enough to generate westward trench motions, which is confirmed by our study. An asymmetric ridge position can affect NR because it creates uneven oceanic plates sizes, and leaves the velocity of the larger plate roughly unchanged compared to a symmetric ridge position (this velocity is controlled by slab dip primarily). Oceanic plates do not thicken past 70 Ma (i.e., when they reach a maximum thickness of 110 km) in our models, which contributes to minimize the dynamic effects of ridge position. The largest plate should otherwise reach ~140 km. *Nagel et al.* [2008] did not account for this effect, although this choice may be appropriate for the Pacific domain [e.g., *Marty and Cazenave*, 1989]. Therefore, based on the results shown in Figure 11, we suggest that westward trench motions are primarily explained by slab properties, instead of ridge properties.

[57] Many of our models contain the same amount of net rotation, while presenting different plate sizes and driving mechanisms. This suggests that, without geological context, the amplitude of net rotation in itself provides little information about the distribution and nature of the forces that are (or were) driving mantle flow. However, when interpreted for a specific tectonic setting such as the Pacific at present-day, studying NR can help understanding which of the local dynamics have an impact on plate motions at a global scale.

[58] In nature, slab dip correlates with trench and upper plate motion [e.g., *Lallemand et al.*, 2005]: steep slabs are more likely to result in trench advance, and shallow slabs in trench retreat. Our models and those of others [*Bellahsen et al.*, 2005; *Faccenna et al.*, 2007; *Di Giuseppe et al.*, 2008; *Stegman et al.*, 2010] show the same behavior, and provide an additional constraint: in order to yield trench advance, slab viscosity should exceed that of the upper mantle by several orders of magnitude. Our models suggest that the ability of steeply dipping slabs to promote trench advance is linked to the pressure and velocity fields that they create in the mantle (cf. Figures 5 and 6). Steep slabs create a unique pattern of almost symmetrical pressures and velocities in both continental and oceanic slab corners: in the oceanic slab corner, the pressure is negative and the mantle flows toward the slab, whereas underneath slabs of average dip, the pressure is positive and the mantle flows away from the slab. This pattern makes the slab hinge advance toward the overriding plate. In the continental slab corner, above the slab, the pressure is also negative, but to a small extent in comparison to a case where the slab is shallow. This results in a lesser suction of the overriding plate toward the slab, therefore a lesser tendency to retreat, facilitating the advance of the steep slab. Also, in contrary to a shallow slab, a steep one generates a relatively smaller return flow, with a tendency to impede the advance of the slab/trench. An alternative explanation has been proposed by *Di Giuseppe et al.* [2008], where stiff slabs are expected to advance because of their inability to unbend at depth. *Heuret and Lallemand* [2005] made the case that natural examples also show a good correlation between trench motions and slab age, and *Di Giuseppe et al.* [2009] have shown numerically that trench behavior is ultimately related to the age of the plate when it subducts. Our study being based on instantaneous modeling, we do not address what creates slab dip asymmetry along the Pacific margins in the first place. Slab dip angles can be explained based on local slab or upper plate properties [e.g., *Royden and Husson*, 2006; *Faccenna et al.*, 2007; *Schellart*, 2008; *Ribe*, 2010]. The models of *Di Giuseppe et al.* [2008, 2009] offer a plausible explanation for slab dip angles based on asymmetric lithospheric ages, which affects the ability of the lithosphere to bend. This interpretation is also key in the study by *Faccenna et al.* [2009] who suggested that the subduction of Mesozoic lithosphere correlates with the recent advance of the Izu-Bonin-Mariana trench system and the speed-up of the Pacific plate. During episodes of rapid NR, plate configuration may evolve toward a slower, more energetically favorable NR, for example through ridge migration (which affects plate size ratio and the age of the subducting seafloor) and slab dip evolution, which can both occur at rates similar to that of plate motions.

[59] In nature, much variations of slab length (and perhaps thickness) are observed, as well as variations of slab dip with depth [e.g., *Heuret and Lallemand*, 2005; *Li et al.*, 2008]. In order to test what effect these local variations may have on our results, we ran models where the slabs stopped at the upper-lower mantle boundary. These models yielded similar trends in term of trench motions and γ, which lends confidence in the robustness of our results.

[60] Our models suggest that the properties of the weak zones between slabs and upper plates exert a major effect on the variety of trench behaviors that can be modeled numerically. Our tests suggest that the weak zones viscosity should not exceed that of the upper mantle in order to model the full range of trench behavior observed at present-day. The WZ thickness required to get the maximum net rotation amplitudes is about 10–20 km with the viscosity contrast that we used. A quantitative assessment of this effect in 3-D could help understanding whether the slow net rotations predicted by numerical studies [e.g., *Becker*, 2006; *Zhong*, 2001] are realistic or result from numerical limitations [*Stadler et al.*, 2010]. Models using non-Newtonian rheologies may require a different resolution and perhaps show different behaviors; however, this is beyond the scope of our study.

[61] Our results suggest two straightforward, potential explanations for the relatively high NR amplitudes that we obtained, in comparison to those in previous numerical models. First, the amplitude of net rotation depends on the partitioning between slab pull and slab suction (section 3.2). This will depend, for instance, on the viscosity of the slabs, and the method used to account for them in the model. When seismic tomography is used as the main source of buoyancy forces in the mantle, slab are not necessarily physically attached to the plates as much as they are in our models, and therefore drive the plates primarily through slab suction. Secondly, weak zones' physical properties seem to play a major role in the maximum NR amplitudes that can be induced, and the coupling between adjacent plates may have been underestimated in

studies where the weak zones exceeded several tenth of kilometers.

5. Conclusions

[62] Slab properties, ridge position, and plate coupling at the trench exert strong controls on the amplitude of net rotation and trench motions. Other lateral variations of viscosity such as a locally weak upper mantle (asthenosphere), and stiff continental keels have smaller effects on NR, but can significantly influence trench motions. Models where the mantle is weaker underneath the oceanic plates than under continents produce trench motions patterns and continental velocities that are closer to the observations. In such models, a simple scaling relationship connects the amount of NR to the size of the oceanic plates, slab dip angles, and the ratio of slab over upper mantle viscosities. Our models generate a very broad range of NR amplitudes as a function of tectonic parameters, which can be linked to evolutionary scenarios for the Pacific basin.

[63] This study emphasizes the links between episodes of rapid net rotation, unidirectional trench motions, rapid ridge migration, and high slab viscosities. Our analysis shows that ridge position affects the size of the plates and therefore, average surface velocity and NR, but this effect is mostly due to surface geometry. Thus, NR is a weak diagnostic of deep dynamics since it can be induced by a process which merely affects deep mantle flow. Slabs, on the contrary, are able to control plate and mantle dynamics. Slab dip, in particular, controls the pressure field in the vicinity of the slab, which is ultimately linked to slab return flow and trench behavior. The viscosity of slabs affects the partitioning between slab pull, which promotes high NR, and slab suction, which promotes low NR.

[64] In most of our models, the ridge migrates in such a way that it reduces NR, potentially stabilizing the global plate tectonic system over time. This suggests that episodes of large NR might only be transient. Asymmetric oceanic plate velocities result in ridge migration, and in that case a basin-centered ridge is not the most stable position. A stable Pacific basin configuration would require either symmetric slab pull forces and ridge position, or asymmetric slab pull forces balanced by an asymmetric ridge position. Our models hint that, as the Pacific domain closes and the Atlantic opens, the East Pacific Rise tends to migrate toward the west, thereby minimizing plate asymmetry. As a result, the net rotation should decrease, and the age

of the subducting lithosphere on each sides of the Pacific tend to even out, which may end the westward motion of some Pacific trenches. At present, slow trench advance in the western Pacific and rapid trench retreat in the eastern Pacific favor such a reequilibration.

Acknowledgments

References

Alpert, L., T. W. Becker, and I. W. Bailey (2010), Global slab deformation and centroid moment constraints on viscosity, *Geochem. Geophys. Geosyst.*, *11*, Q12006, doi:10.1029/2010GC003301.

Becker, T. W. (2006), On the effect of temperature and strain-rate dependent viscosity on global mantle flow, net rotation, and plate-driving forces, *Geophys. J. Int.*, *167*, 943–957.

Becker, T. W. (2008a), Azimuthal seismic anisotropy constrains net rotation of the lithosphere, *Geophys. Res. Lett.*, *35*, L05303, doi:10.1029/2007GL032928.

Becker, T. W. (2008b), Correction to "Azimuthal seismic anisotropy constrains net rotation of the lithosphere," *Geophys. Res. Lett.*, *35*, L08308, doi:10.1029/2008GL033946.

Becker, T. W., and C. Faccenna (2009), A review of the role of subduction dynamics for regional and global plate motions, in *Subduction Zone Geodynamics*, edited by F. Funiciello and S. Lallemand, pp. 3–34, Springer, Berlin.

Becker, T. W., and H. Kawakatsu (2011), On the role of anisotropic viscosity for plate-scale flow, *Geophys. Res. Lett.*, *38*, L17307, doi:10.1029/2011GL048584.

Becker, T. W., and R. J. O'Connell (2001), Predicting plate velocities with mantle circulation models, *Geochem. Geophys. Geosyst.*, *2*(12), 1060, doi:10.1029/2001GC000171.

Bellahsen, N., C. Faccenna, and F. Funiciello (2005), Dynamics of subduction and plate motion in laboratory experiments: Insights into the "plate tectonics" behavior of the Earth, *J. Geophys. Res.*, *110*, B01401, doi:10.1029/2004JB002999.

Bercovici, D., Y. Ricard, and M. Richards (2000), The relationship between mantle dynamics and plate tectonics: A primer, in *The History and Dynamics of Global Plate Motions*, *Geophys. Monogr. Ser.*, vol. 121, edited by M. Richards, R. Gordon, and R. D. van der Hilst, pp. 5–46, AGU, Washington, D. C.

Billen, M. I. (2008), Modeling the dynamics of subducting slabs, *Annu. Rev. Earth Planet. Sci.*, *36*, 325–356.

Billen, M. I., and M. Jadamec (2012), Origin of localized fast mantle flow velocity in numerical models of subduction, *Geochem. Geophys. Geosyst.*, *13*, Q01016, doi:10.1029/2011GC003856.

Bostrom, R. (1971), Westward displacement of the lithosphere, *Nature*, *234*, 536–538.

Čadek, O., and L. Fleitout (2003), Effect of lateral viscosity variations in the top 300 km of the mantle on the geoid and dynamic topography, *Geophys. J. Int.*, *152*, 566–580.

Čadek, O., H. Cizkova, and D. A. Yuen (1997), Can long-wavelength dynamical signatures be compatible with layered mantle convection?, *Geophys. Res. Lett.*, *16*, 2091–2094.

Capitanio, F., G. Morra, and S. Goes (2009), Dynamics of plate bending at the trench and slab-plate coupling, *Geochem. Geophys. Geosyst.*, *10*, Q04002, doi:10.1029/2008GC002348.

Conrad, C. P., and M. Behn (2010), Constraints on lithosphere net rotation and asthenospheric viscosity from global mantle flow models and seismic anisotropy, *Geochem. Geophys. Geosyst.*, *11*, Q05W05, doi:10.1029/2009GC002970.

Conrad, C. P., and C. Lithgow-Bertelloni (2002), How mantle slabs drive plate tectonics, *Science*, *298*, 207–209.

Conrad, C. P., and C. Lithgow-Bertelloni (2004), The temporal evolution of plate driving forces: Importance of "slab suction" versus "slab pull" during the Cenozoic, *J. Geophys. Res.*, *109*, B10407, doi:10.1029/2004JB002991.

Conrad, C. P., and C. Lithgow-Bertelloni (2006), Influence of continental roots and asthenosphere on plate-mantle coupling, *Geophys. Res. Lett.*, *33*, L05312, doi:10.1029/2005GL025621.

Crespi, M., M. Cuffaro, C. Doglioni, F. Giannone, and F. Riguzzi (2007), Space geodesy validation of the global lithospheric flow, *Geophys. J. Int.*, *168*, 491–506.

Dabrowski, M., M. Krotkiewski, and D. W. Schmid (2008), MILAMIN: MATLAB-based finite element method solver for large problems, *Geochem. Geophys. Geosyst.*, *9*, Q04030, doi:10.1029/2007GC001719.

Di Giuseppe, E., J. van Hunen, F. Funiciello, C. Faccenna, and D. Giardini (2008), Slab stiffness controls trench motion: Insights from numerical models, *Geochem. Geophys. Geosyst.*, *9*, Q02014, doi:10.1029/2007GC001776.

Di Giuseppe, E., C. Faccenna, F. Funiciello, J. van Hunen, and D. Giardini (2009), On the relation between trench migration, seafloor age, and the strength of the subducting lithosphere, *Lithosphere*, *1*, 121–128.

Doglioni, C., E. Carminati, M. Cuffaro, and D. Scrocca (2007), Subduction kinematics and dynamic constraints, *Earth Sci. Rev.*, *83*, 125–175.

Enns, A., T. W. Becker, and H. Schmeling (2005), The dynamics of subduction and trench migration for viscosity stratification, *Geophys. J. Int.*, *160*, 761–775.

Faccenna, C., A. Heuret, F. Funiciello, S. Lallemand, and T. W. Becker (2007), Predicting trench and plate motion from the dynamics of a strong slab, *Earth Planet. Sci. Lett.*, *257*, 29–36.

Faccenna, C., E. Di Giuseppe, F. Funiciello, S. Lallemand, and J. van Hunen (2009), Control of seafloor aging on the migration of the Izu-Bonin-Mariana Trench, *Earth Planet. Sci. Lett.*, *288*, 386–398.

Forsyth, D. W., and S. Uyeda (1975), On the relative importance of the driving forces of plate motion, *Geophys. J. R. Astron. Soc.*, *43*, 163–200.

Funiciello, F., C. Faccenna, D. Giardini, and K. Regenauer-Lieb (2003), Dynamics of retreating slabs: 2. Insights from three-dimensional laboratory experiments, *J. Geophys. Res.*, *108*(B4), 2207, doi:10.1029/2001JB000896.

Funiciello, F., C. Faccenna, and D. Giardini (2004), Flow in the evolution of subduction system: Insights from 3-D laboratory experiments, *Geophys. J. Int.*, *157*, 1393–1407.

Funiciello, F., C. Faccenna, A. Heuret, E. Di Giuseppe, S. Lallemand, and T. W. Becker (2008), Trench migration, net rotation and slab-mantle coupling, *Earth Planet. Sci. Lett.*, *271*, 233–240.

Gordon, R. G., and D. M. Jurdy (1986), Cenozoic global plate motions, *J. Geophys. Res.*, *91*, 12,389–12,406.

Gripp, A. E., and R. G. Gordon (2002), Young tracks of hotspots and current plate velocities, *Geophys. J. Int.*, *150*, 321–361.

Gurnis, M., and T. Torsvik (1994), Rapid drift of large continents during the Late Precambrian and Paleozoic: Paleomagnetic constraints and dynamics models, *Geology*, *22*, 1023–1026.

Hager, B. H., and R. J. O'Connell (1978), Subduction zone dip angles and flow derived by plate motion, *Tectonophysics*, *50*, 111–133.

Heuret, A., and S. Lallemand (2005), Slab dynamics and back-arc deformation, *Phys. Earth Planet. Inter.*, *149*, 31–51.

Hoink, T., and A. Lenardic (2008), Three-dimensional mantle convection simulations with a low viscosity asthenosphere and the relationship between heat flow and the horizontal length scale of convection, *Geophys. Res. Lett.*, *35*, L10304, doi:10.1029/2008GL033854.

Hoink, T., and A. Lenardic (2010), Long wavelength convection, Poiseuille-Couette flow in the low-viscosity asthenosphere and the strength of plate margins, *Geophys. J. Int.*, *180*, 23–33.

Husson, L., C. P. Conrad, and C. Faccenna (2008), Tethyan closure, Andean orogeny, and westward drift of the Pacific Basin, *Earth Planet. Sci. Lett.*, *271*, 303–310.

Jordan, T. H. (1974), Some comments on tidal drag as a mechanism for driving plate motions, *J. Geophys. Res.*, *79*, 2141–2142.

Jordan, T. (1975), The continental tectosphere, *Rev. Geophys.*, *13*, 1–12.

Jordan, T. (1988), Structure and formation of the continental tectosphere, *J. Petrol.*, *Special Volume 1988*, 11–37.

King, S. D., and B. H. Hager (1990), The relationship between plate velocity and trench viscosity in Newtonian and power-law subduction calculations, *Geophys. Res. Lett.*, *17*, 2409–2412.

King, S. D., C. W. Gable, and S. A. Weinstein (1992), Models of convection-driven tectonic plates: A comparison of methods and results, *Geophys. J. Int.*, *109*, 481–487.

Kreemer, C. (2009), Absolute plate motions constrained by shear wave splitting orientations with implications for hot spot motions and mantle flow, *J. Geophys. Res.*, *114*, B10405, doi:10.1029/2009JB006416.

Lallemand, S., A. Heuret, and D. Boutelier (2005), On the relationships between slab dip, back-arc stress, upper plate absolute motion, and crustal nature in subduction zones, *Geochem. Geophys. Geosyst.*, *6*, Q09006, doi:10.1029/2005GC000917.

Li, C., R. D. van der Hilst, E. R. Engdahl, and S. Burdick (2008), A new global model for P wave speed variations in Earth's mantle, *Geochem. Geophys. Geosyst.*, *9*, Q05018, doi:10.1029/2007GC001806.

Lithgow-Bertelloni, C., and M. A. Richards (1998), The dynamics of Cenozoic and Mesozoic plate motions, *Rev. Geophys.*, *36*, 27–78.

Marty, J. C., and A. Cazenave (1989), Regional variations in subsidence rate of oceanic plates: A global analysis, *Earth Planet. Sci. Lett.*, *94*, 301–315.

McKenzie, D. P. (1979), Finite deformation during fluid flow, *Geophys. J. R. Astron. Soc.*, *58*, 689–715.

Minster, J. B., T. H. Jordan, P. Molnar, and E. Haines (1974), Numerical modelling of instantaneous plate tectonics, *Geophys. J. R. Astron. Soc.*, *36*, 541–576.

Morgan, J. P. (1971), Convection plumes in the lower mantle, *Nature*, *230*, 42–43.

Nagel, T. J., W. B. F. Ryan, A. Malinverno, and W. R. Buck (2008), Pacific trench motions controlled by the asymmetric plate configuration, *Tectonics*, *27*, TC3005, doi:10.1029/2007TC002183.

O'Connell, R. J., C. W. Gable, and B. H. Hager (1991), Toroidal-poloidal partitioning of lithospheric plate motions, in *Glacial Isostasy, Sea-Level and Mantle Rheology*, edited by R. Sabadini and K. Lambeck, pp. 535–551, Kluwer Acad., Norwell, Mass.

O'Driscoll, L., E. Humphreys, and F. Saucier (2009), Subduction adjacent to deep continental roots: Enhanced negative pressure in the mantle wedge, mountain building and continental motion, *Earth Planet. Sci. Lett.*, *280*, 61–70.

Olson, P., and D. Bercovici (1991), On the equipartitioning of kinematic energy in plate tectonics, *Geophys. Res. Lett.*, *18*, 1751–1754.

O'Neill, C., D. Müller, and B. Steinberger (2005), On the uncertainties in hot spot reconstructions and the significance of moving hot spot reference frames, *Geochem. Geophys. Geosyst.*, *6*, Q04003, doi:10.1029/2004GC000784.

Piromallo, P., T. W. Becker, F. Funiciello, and C. Faccenna (2006), Three-dimensional instantaneous mantle flow induced by subduction, *Geophys. Res. Lett.*, *33*, L08304, doi:10.1029/2005GL025390.

Ramos, V., E. Cristallini, and D. Pérez (2002), The Pampean flat-slab of the central Andes, *J. South Am. Earth Sci.*, *15*, 59–78.

Ranalli, G. (2000), Westward drift of the lithosphere: Not a result of rotational drag, *Geophys. J. Int.*, *141*, 535–537.

Ribe, N. M. (1992), The dynamics of thin shells with variable viscosity and the origin of toroidal flow in the mantle, *Geophys. J. Int.*, *110*, 537–552.

Ribe, N. (2010), Bending mechanics and mode selection in free subduction: A thin-sheet analysis, *Geophys. J. Int.*, *180*, 559–576.

Ricard, Y., and C. Vigny (1989), Mantle dynamics with induced plate tectonics, *J. Geophys. Res.*, *94*, 17,543–17,559.

Ricard, Y., C. Doglioni, and R. Sabadini (1991), Differential rotation between lithosphere and mantle: A consequence of lateral mantle viscosity variations, *J. Geophys. Res.*, *96*, 8407–8415.

Ricard, Y., M. A. Richards, C. Lithgow-Bertelloni, and Y. Le Stunff (1993), A geodynamic model of mantle density heterogeneity, *J. Geophys. Res.*, *98*, 21,895–21,909.

Royden, L. H., and L. Husson (2006), Trench motion, slab geometry and viscous stresses in subduction systems, *Geophys. J. Int.*, *167*, 881–905.

Schellart, W. P. (2008), Kinematics and flow patterns in deep mantle and upper mantle subduction models: Influence of the mantle depth and slab to mantle viscosity ratio, *Geochem. Geophys. Geosyst.*, *9*, Q03014, doi:10.1029/2007GC001656.

Schellart, W. P., J. Freeman, D. R. Stegman, and L. N. Moresi (2007), Evolution and diversity of subduction zones controlled by slab width, *Nature*, *446*, 308–311.

Schellart, W., D. Stegman, and J. Freeman (2008), Global trench migration velocities and slab migration induced upper mantle volume fluxes: Constraints to find an earth reference frame based on minimizing viscous dissipation, *Earth Sci. Rev.*, *88*, 118–144.

Scoppola, B., D. Boccaletti, M. Bevis, E. Carminati, and C. Doglioni (2006), The westward drift of the lithosphere: A rotational drag?, *Geol. Soc. Am. Bull.*, *118*, 199–209, doi:10.1130/B25734.1.

Stadler, G., M. Gurnis, C. Burstedde, L. C. Wilcox, L. Alisic, and O. Ghattas (2010), The dynamics of plate tectonics and

mantle flow: From local to global scales, *Science*, *329*, 1033–1038.

Stegman, D. R., R. Farrington, F. A. Capitanio, and W. P. Schellart (2010), A regime diagram for subduction styles from 3-D numerical models of free subduction, *Tectonophysics*, *483*, 29–45.

Steinberger, B. (2000), Slabs in the lower mantle—Results of dynamic modelling compared with tomographic images and the geoid, *Phys. Earth Planet. Inter.*, *118*, 241–257.

Steinberger, B., R. Sutherland, and R. J. O'Connell (2004), Prediction of Emperor-Hawaii seamount locations from a revised model of global plate motion and mantle flow, *Nature*, *430*, 167–173.

Tackley, P. J. (2000a), Self-consistent generation of tectonic plates in time-dependent, three-dimensional mantle convection simulations: 1. Pseudoplastic yielding, *Geochem. Geophys. Geosyst.*, *1*(8), 1021, doi:10.1029/2000GC000036.

Tackley, P. J. (2000b), Self-consistent generation of tectonic plates in time-dependent, three-dimensional mantle convection simulations: 2. Strain weakening and asthenosphere, *Geochem. Geophys. Geosyst.*, *1*(8), 1026, doi:10.1029/2000GC000043.

Torsvik, T., B. Steinberger, M. Gurnis, and C. Gaina (2010), Plate tectonics and net lithosphere rotation over the past 150 my, *Earth Planet. Sci. Lett.*, *291*, 106–112.

Tovish, A., and G. Schubert (1978), Island arc curvature, velocity of continents and angle of subduction, *Geophys. Res. Lett.*, *5*, 329–332.

Turcotte, D. L., and E. R. Oxburgh (1967), Finite amplitude convective cells and continental drift, *J. Fluid Mech.*, *28*, 29–42.

Turcotte, D. L., and G. Schubert (2002), *Geodynamics*, 2nd ed., Cambridge Univ. Press, Cambridge, U. K.

Uyeda, S., and H. J. Kanamori (1979), Back-arc opening and the mode of subduction, *J. Geophys. Res.*, *84*, 1049–1061.

van der Meer, D. G., W. Spakman, D. J. J. van Hinsbergen, M. L. Amaru, and T. H. Torsvik (2010), Towards absolute plate motions constrained by lower-mantle slab remnants, *Nat. Geosci.*, *3*, 36–40.

van Summeren, J., C. Conrad, and C. Lithgow-Bertelloni (2012), The importance of weak slabs and a global asthenosphere to plate motions, *Geochem. Geophys. Geosyst.*, *13*, Q0AK03, doi:10.1029/2011GC003873.

Wegener, A. (1924), *The Origin of Continents and Oceans*, Methuen, London.

Weinstein, S., and P. Olson (1992), Thermal convection with non-Newtonian plates, *Geophys. J. Int.*, *111*, 515–530.

Wen, L., and D. L. Anderson (1997), Present-day plate motion constraint on mantle rheology and convection, *J. Geophys. Res.*, *102*, 24,639–24,653.

Zhang, S., and U. Christensen (1993), Some effects of lateral viscosity variations on geoid and surface velocities induced by density anomalies in the mantle, *Geophys. J. Int.*, *114*, 531–547.

Zheng, L., R. G. Gordon, D. Argus, C. DeMets, and C. W. Kreemer (2010), Current plate motion relative to the hotspots and to the mantle, Abstract GP24A-07 presented at 2010 Fall Meeting, AGU, San Francisco, Calif., 13–17 Dec.

Zhong, S. (2001), Role of ocean-continent contrast and continental keels on plate motion, net rotation of lithosphere, and the geoid, *J. Geophys. Res.*, *106*, 703–712.

Zhong, S., and M. Gurnis (1995), Mantle convection with plates and mobile, faulted plate margins, *Science*, *267*, 838–842.